SANDIA REPORT
SAND2022-7375
Printed June 2022

Sandia National Laboratories

Stochastic Modeling in a Multimaterial Continuum Mixture Shock Physics Code

Shane C. Schumacher and Melvin R. Baer

Prepared by
Sandia National Laboratories
Albuquerque, New Mexico
87185 and Livermore,
California 94550

Issued by Sandia National Laboratories, operated for the United States Department of Energy by National Technology & Engineering Solutions of Sandia, LLC.

Available to DOE and DOE contractors from
U.S. Department of Energy
Office of Scientific and Technical Information
P.O. Box 62
Oak Ridge, TN 37831

Telephone: (865) 576-8401
Facsimile: (865) 576-5728
E-Mail: reports@osti.gov
Online ordering: http://www.osti.gov/scitech

Available to the public from
U.S. Department of Commerce
National Technical Information Service
5301 Shawnee Rd
Alexandria, VA 22312

Telephone: (800) 553-6847
Facsimile: (703) 605-6900
E-Mail: orders@ntis.gov
Online order: https://classic.ntis.gov/help/order-methods/

ABSTRACT

Stochastic modelling approaches are presented to capture random effects at multiple time and length scales. Random processes that occur at the microscale produce nondeterministic effects at the macroscale. Here we present three stochastic modeling approaches that describe random processes at microscopic length scales and map these processes to the macroscopic length scale. The first stochastic modeling approach is based upon a particle based numerical technique to solve a Stochastic Differential Equation (SDE) using an arbitrary diffusion process to capture random processes at the microstructural level. The second approach prescribes a Probability Density Function (PDF) for the drift and diffusion of the random variable derived using the forward and backward Kolmogorov equations. This method requires mean and drift evolution PDF transport equations. The third approach is the coupling of multiple random variables which are dependent on each other. The relationship of the PDFs and a coupling function, known as a copula, produces a Joint Probability Density Function (JPDF). These stochastic modeling approaches are implemented into a Multiple Component (MC) shock physics computational code and used to model statistical fracture and reactive flow applications.

CONTENTS

Abstract....3
Acronyms and Terms....7
1. Introduction....11
2. General Numerical Support for Incoporating Stochastics in Multiple Component Shock Physics....15
   2.1. General Formalism....15
   2.2. Stochastic Particle Method....16
   2.3. Particle Motion....19
   2.4. Adaptive Particle Insertion and Deletion....21
3. Stochastic Particle Method Using Arbitrary Diffusion....23
   3.1. Description....23
   3.2. Example: Stochastic Damage....23
   3.3. Result....24
4. Stochastic Particle Method Based Upon Forward/Backward Kolmogorov Methods....29
   4.1. Forward/Backward Kolmogorov with Stochastic Models of Drift and Diffusion....29
      4.1.1. Normal/Gaussian....30
      4.1.2. Weibull....30
      4.1.3. Frechet....30
      4.1.4. Generalized Extremum....30
   4.2. Example: Stochastic Reactive Flow....31
   4.3. Result....33
5. Stochastic Modeling Method for Joint Probability Density Functions....37
   5.1. Copula....38
   5.2. Example: Stochastic Reactive Flow with Damage....39
   5.3. Result....42
6. Conclusion....54
References....55
Distribution....57

LIST OF FIGURES

Figure 2-1. Example of particle binning to generate probability density function....17
Figure 2-2. Particle face velocity interpolation and position update....20
Figure 2-3. Particle vertex velocity interpolation and position update....20
Figure 3-1. Symmetric copper-copper impact....25
Figure 3-2. Mean fracture stress for symmetric copper-copper impact....25
Figure 3-3. Fracture location for symmetric copper-copper impact....26
Figure 3-4. Fracture time for symmetric copper-copper impact....26
Figure 4-1. Piston impact of distended energetic material....33
Figure 4-2. Fréchet probability density function initial state....34
Figure 4-3. Gas Temperature at ignition of Bullseye with piston velocity at 150 m/s....35
Figure 4-4. Ignition time of Bullseye with piston velocity at 150 m/s....35
Figure 4-5. Ignition location of Bullseye with piston velocity at 150 m/s....36
Figure 5-1. Piston impact of Composition B energetic material....43
Figure 5-2. Fréchet probability density function initial state....43
Figure 5-3. Weibull probability density function initial state....44
Figure 5-4. Tension failure model calibration (data in blue and the model fit in orange)....44
Figure 5-5. Compression failure model calibration (data in blue and the model fit in orange)....45
Figure 5-6. Gas Temperature at ignition of Composition B with piston velocity at 250 m/s....45
Figure 5-7. Ignition time of Composition B with piston velocity at 250 m/s....46
Figure 5-8. Ignition location of Composition B with piston velocity at 250 m/s....46
Figure 5-9. Damage state at ignition of Composition B with piston velocity at 250 m/s....47
Figure 5-10. initial JPDF for Composition B....48
Figure 5-11. JPDF for Composition B at 60e-6 seconds....48
Figure 5-12. JPDF for Composition B at 79.2e-6 seconds....49
Figure 5-13. Magnified JPDF for Composition B at 79.2e-6 seconds....49
Figure 5-14. Gas Temperature at ignition of Composition B with piston velocity at 250 m/s without damage modeling....50
Figure 5-15. Ignition time of Composition B with piston velocity at 250 m/s without damage modeling....51
Figure 5-12. Ignition location of Composition B with piston velocity at 250 m/s without damage modeling....51

LIST OF TABLES

Table 5-1 Kinetic Theory of Fracture parameters for Composition B 44
Table 5-2 JPDF model coefficients at ignition 47

ACRONYMS AND TERMS

Acronym/Term	Definition
MC	Multiple Component
PDF	Probability Density Function
JPDF	Joint Probability Density Function
SDE	Stochastic Differential Equation
LDRD	Laboratory Directed Research and Development
DMGIR	DaMaGe Induced Reaction
ϖ	Random variable
ς	Random variable
τ	Time
$\Delta\tau$	Change in time (timestep)
τ_s	Time scale based on random variable interactions at the microscale
$\boldsymbol{dft}_i(x_\tau,\tau)$	Drift function based in time
$\boldsymbol{Dif}_{ij}(x_\tau,\tau)$	Diffusion tensor based in time
t	Scaled time
$\mathbf{g}$	Drift vector based in scaled time
$\mathbf{H}$	Diffusion tensor based in scaled time
$\mathbf{h}$	Diffusion vector based in scaled time
g	Drift scalar function based in scaled time
g_t	Derivative of drift function w.r.t. scaled time t
h	Diffusion scalar function based in scaled time
B	Random process
μ	Mean
σ^2	Variance
σ	Standard deviation ($\sigma = \sqrt{\sigma^2}$)
nb	Number of bins
Δbin	Bin size
np_i	Number of particles in a bin
npt	Total number of particles in all bins
$g(x)$	Arbitrary function of the random variable
$f(x)$	Probability Density Function (PDF)
$\langle g \rangle$	Mean quantity of the function $g(x)$
$\boldsymbol{v}^p$	Velocity vector on the particle
$\boldsymbol{v}^f$	Velocity vector at the cell face

Acronym/Term	Definition
$\boldsymbol{v}^{vtx}$	Velocity vector at the vertex
$\boldsymbol{pos}$	Position vector of particle
$\boldsymbol{pos^0}$	Initial position of particle vector
$\boldsymbol{cell\_length}$	Cell size vector
ξ	Random number
k_1	Diffusion calibration coefficients 1
k_2	Diffusion calibration coefficient 2
$\mathbb{D}$	Damage random variable
$\mathbb{D}_0$	Constant n_0=1.58
τ_0	Time constant
k	Boltzmann's constant
T	Temperature
U	Calibration coefficient
γ	Calibration coefficient
A	Avogadro's number
S	Stress
k_w	Weibull constant
λ_w	Weibull constant
$\langle F \rangle$	Mean fracture stress
F	Fracture stress
$\langle C_p \rangle$	Mean specific heat
A	Calibration coefficient
E_a	Activation energy
ΔH_{rel}	Change is energy due to reaction
R	Gas constant
α	Thermal diffusivity
C_1	Diffusion model calibration coefficient
C_2	Diffusion model calibration coefficient
$\langle T \rangle$	Mean temperature
$\langle \sigma_T^2 \rangle$	Mean temperature variance
m_w	Weibull PDF calibration coefficient
α_F	Fréchet PDF calibration coefficient
m_F	Fréchet PDF calibration coefficient
s_F	Fréchet PDF calibration coefficient

Acronym/Term	Definition
α_E	Extremum PDF calibration coefficient
m_E	Extremum PDF calibration coefficient
s_E	Extremum PDF calibration coefficient
$F(x,y)$	Multivariant Cumulative Distribution Function (CDF)
$JCDF(x,y)$	Joint CDF (JCDF)
$F_x(x)$	Marginal CDF of random variable x
$F_y(y)$	Marginal CDF of random variable y
$f(x,y)$	Bivariant Joint Probability Density Function (JPDF)
$f_x(x)$	Marginal PDF of random variable x
$f_y(y)$	Marginal PDF of random variable y
corr	JPDF correlation coefficient
ϑ	Coupling parameter
μ_x	Mean of random variable x
μ_y	Mean of random variable y
σ_x^2	Variance of random variable x
σ_y^2	Variance of random variable y
σ_{xy}^2	Covariance
$F(x)$	CDF of random variable x
$F(y)$	CDF of random variable y
ϑ	Coupling parameter
$f(x)$	PDF of random variable x
$f(y)$	PDF of random variable y
λ	Reaction progress random variable
C_s^+	Mass exchange rate for the condensed (solid) phase
T_0	Initial temperature
γ_s	True density of the condensed (solid) phase
C_p	Specific heat at constant pressure
$B_{\mathbb{D}}$	Surface damage model coefficient
$m_{\mathbb{D}}$	Surface damage model exponential coefficient
$k_{\mathbb{D}1}$	Damage diffusion model coefficient
$k_{\mathbb{D}2}$	Damage diffusion model coefficient
$k_{\lambda 1}$	Reaction diffusion model coefficient
$k_{\lambda 2}$	Reaction diffusion model coefficient

1. INTRODUCTION

Stochastic modeling may be applied to describe the evolution of a family of random variables that are associated with a nondeterministic process. Fokker-Plank equations, also known as forward/backward Kolmogorov relationships, form the basis of the modeling approach whereby probability distribution functions (PDFs) of random variables are transported. The Kolmogorov equations are expressed as high dimensional transport equations that are functions of space and time, as well as the random variables themselves. A direct numerical integration of the Kolmogorov equations is prohibitively expensive, and alternative methods are sought to resolve the PDFs. Here, the nondeterministic processes of interest originate from the random material microstructures, that are found at lower length scales below the scale of the desired (i.e., macroscale) numerical simulations.

Heterogenous materials, such as particle-composite matrix materials, granular powder beds, or porous metals to name a few examples, are inherently random due to their microstructure. Thus, any measurement in these materials must recognize the uncertainties associated with the statistical nature of the microstructure. The focus of this effort is the incorporation of microstructure effects that greatly influence the macroscopic behavior of the material response. The microstructural characteristics are due to the random features such as grain structure, grain size, porosity, etc. These random features influence the macroscopic behavior causing variations in the macroscopic variables (random variables) such as temperature or stress. Relating the microstructural random features to the macroscopic variables is accomplished by utilizing stochastic computational methods.

As an example of this stochastic modeling approach, consider the shock initiation of a heterogenous energetic material near the threshold of self-sustaining reactive behavior [1]. At weak conditions, the onset to reaction is statistical due to the random nature of the microstructure of the reactive material. Uncertainty in the local composition and geometry introduces randomness of the reactive process. It is well known that energy localization effects produce thermally activated sites known as "hot-spots" and the evolution or growth of reaction is greatly dependent on specific surface area of the heterogenous material. When energy addition exceeds the dissipative processes, ignition occurs, and reactive waves are generated. As the reaction wave propagates and becomes self-sustaining, a reaction wave can transition to a detonation wave. Hence, the microstructure of energetic materials has a dominate role in determining the threshold of ignition and the resulting energetic performance.

Another example of the stochastic modeling approach considers the fracture of materials [2]. The fracture mechanics of materials is controlled by the uncertainty of the microstructure of the material, grain bonding, crystalline structure, grain size, etc. These random microstructural features in the heterogenous material dictate the macroscopic fracture process. When a grain bond or grain crystal fractures, a microcrack is formed. Several microcracks will form within the microstructure at random crystal or grain boundaries. As the microcracks coalesce, they can form a macrocrack resulting in macroscopic failure leading to a decrease in the material stress. The role of the microstructure has a dominate role in the rate and how the material fractures.

Another example of the stochastic modeling approach considers a specific type of material manufacturing process, namely additive manufacturing (AM) [3]. Additive manufacturing can be used to reduce the manufacturing cost and time of complex parts, using one of many techniques. The wire-fed AM process for metals deposits feed stock material and further bonds it together via welding. The microstructure of these additive manufactured parts is unique; the bonding process controls the strength of the bonded particles as well as the amount of porosity in the materials. The uncertainty in the porosity of the additive manufactured process is greater than if the material was pressed, forged, or cast. The increase in porosity at the microstructural level controls the macroscopic fracture

response. The porosity in the material creates stress concentrations within the microstructure. At the boundaries of the porosity or particle bonds, the stresses are the greatest and break forming microcracks. Several microcracks will form and result in the formation of a macrocrack. Once again, the role of the microstructure has a dominate role in the macroscopic response of the material.

To characterize the nondeterministic processes occurring at the microstructural level of a material, two methods are typically used. The first method requires repeated experiments to assess the statistical nature of the random variable, thus generating the necessary data to determine and characterize a PDF. A second method uses a combination of repeated experiments with computational methods. Just as in the first method, the goal of the combined computational-experimental approach is to determine and characterize a PDF of the random variable. This method is typically used when direct measurements at the microstructure or directly measuring the random variable are not possible. A Representative Volume Element (RVE) or similar model of the microstructure is generated, where mean and variance states of the random variable(s) are determined. The macroscopic response is compared to the measured data from multiple experiments [1,4]. Using the results from either two methods, the random features are captured by a constitutive model characterizing the material response. This is accomplished using a PDF of a characterization parameter, or a similar technique that is specific to the constitutive model. Examples of the application of such a technique for heterogeneous materials is given in [5].

In this work, the stochastic computational methods are used to describe the constitutive behavior of a material. The use of stochastic methods in computational tools has been made computationally possible with the introduction of particle methods to solve stochastic differential equations [6]. Using a particle technique, three different stochastic numerical methods have been implemented into the Multiple Component (MC) shock physics computational code [7].

The initial approach builds directly upon the work that was previously performed under a Sandia Laboratory Directed Research and Development (LDRD) project [8]. This method investigated the effect of a stochastic random variable using an arbitrary diffusion function to describe the stochastic nature of a shock-induced reaction. The primary goal of this method is to determine the PDF that describes the stochastic nature of the random variable. Upon determination of the PDF form, an estimate of mean and variance states can be performed.

The second stochastic modeling approach builds upon a method whereby a prescribed PDF is used to describe the stochastic nature of the random variable. In this method, a PDF form is prescribed to evolve the state of the random variable. This method has two advantages, the PDF of the random variable is preserved during the simulation, which results in a reduction of storage memory and computational resources to maintain the stochastic nature of the random variable. This approach uses the forward and reverse Kolmogorov equations to derive models for the drift (mean) and diffusion that are associated with the evolution of the random variable [9]. Here, there are two definitions of the drift and diffusion models, i.e., stationary and non-stationary. Stationary does not permit the drift and diffusion functions to evolve over time, whereas non-stationary allows temporal variation of the drift and diffusion functions. When using the non-stationary modeling approach, additional equations are needed to determine the drift and diffusion processes.

The third stochastic modeling approach is the combination of multiple stochastic random variables that are coupled to each other. This process creates a Joint Probability Density Function (JPDF) that uses a copula joining various PDFs. This method accepts any PDF, and the copula is the defining feature that generates the JPDF. There are several different forms of copulas [10,12] and the use of methods one and two will help determine the form of the copula needed for the simulation. The

combination of the copula, PDF's and choice of random variables makes the JPDF application specific.

Each of the modeling approaches are described in the following four chapters. Chapter two outlines the general stochastic modeling approach to set a basis for the proceeding chapters. Chapter three describes the first stochastic modeling method with an application to fracture mechanics. Chapter four describes the second stochastic modeling method with an application to energetic ignition and performance. Chapter five describes the third stochastic modeling method by coupling fracture and energetic ignition into a JPDF.

This page intentionally left blank

2. GENERAL NUMERICAL SUPPORT FOR INCOPORATING STOCHASTICS IN MULTIPLE COMPONENT SHOCK PHYSICS

This section describes the general formalism of stochastic methods, as developed and implemented into the computational shock physics code Multiple Component (MC) [7]. This provides a general stochastic approach and the infrastructure for modeling random variables at the microscopic length scale that are averaged at the macroscopic length scale (i.e., the scale of the calculation). The statistical effects are characterized by a Probability Density Function (PDF) of a random variable that is incorporated into a constitutive material model. Three stochastic modeling methods will be discussed in this section. Note: lower case letter/text and bold is a vector, upper case letter/text and bold is a tensor and all others are scalars.

2.1. General Formalism

In this study we present modeling stochastic processes based on the temporal and spatial evolution of a Probability Density Function (PDF) based on a Fokker-Planck relationship [1]. This is also known as the forward Kolmogorov equation [13]. In terms of N-random variables the transport equation for the PDF, $f(\boldsymbol{\varpi},\tau)$ is given as:

$$\frac{\partial}{\partial\tau}f(\boldsymbol{\varpi},\tau) = -\sum_{i=1}^{N}\frac{\partial}{\partial\varpi_i}[\boldsymbol{dft}_i(\boldsymbol{\varpi},\tau)f(\boldsymbol{\varpi},\tau)] + \sum_{i=1}^{N}\sum_{j=1}^{N}\frac{\partial^2}{\partial\varpi_i\partial\varpi_j}\left[\boldsymbol{Dif}_{ij}(\boldsymbol{\varpi},\tau)f(\boldsymbol{\varpi},\tau)\right], \quad (2.1.1)$$

where $\boldsymbol{\varpi}$ is a vector of random variables, τ is time and $\boldsymbol{dft}_i(\boldsymbol{\varpi},\tau)$ is a drift vector of random variables. $\boldsymbol{Dif}_{ij}(\boldsymbol{\varpi},\tau)$ is a diffusion tensor. The above equation is scaled in time by a time scale, τ_s. The time scale is necessary to capture the random interactions at the microstructure level, therefore τ becomes t, scaled time, where $t = \frac{\tau}{\tau_s}$. Equation 2.1.1 is rewritten as,

$$\frac{\partial}{\partial t}f(\boldsymbol{\varpi},t) = -\sum_{i=1}^{N}\frac{\partial}{\partial\varpi_i}[\boldsymbol{g}_i(\boldsymbol{\varpi},t)f(\boldsymbol{\varpi},t)] + \sum_{i=1}^{N}\sum_{j=1}^{N}\frac{\partial^2}{\partial\varpi_i\partial\varpi_j}\left[\boldsymbol{H}_{ij}(\boldsymbol{\varpi},t)f(\boldsymbol{\varpi},t)\right] \quad (2.1.2)$$

where $\boldsymbol{g}_i(\boldsymbol{\varpi},t)$ is a drift vector, $f(\boldsymbol{\varpi},t)$ is the PDF in time and $\boldsymbol{H}_{ij}(\boldsymbol{\varpi},t)$ is a diffusion tensor given by:

$$\boldsymbol{H}_{ij}(\boldsymbol{\varpi},t) \triangleq \frac{1}{2}\sum_{k=1}^{M}\boldsymbol{h}_{ik}(\boldsymbol{\varpi},t)\boldsymbol{h}_{kj}(\boldsymbol{\varpi},t), \quad (2.1.3)$$

where $\boldsymbol{h_i}(\boldsymbol{\varpi},t)$ is a diffusion vector and M is the dimension of the diffusion process, i.e. Brownian motion. The scaled time, *t*, is of the scale of the randomness defined by the microstructure. Note that the above transport equation is a function of the spatial coordinates and the set of random variables, as one might expect, a numerical solution can be computationally expensive. An alternative equivalent equation is determined using stochastic calculus and is given by the set of Stochastic Differential Equations (SDEs):

$$d\varpi = g_t(\varpi,t)dt + h(\varpi,t)dB_t, \quad (2.1.4)$$

where $g_t(\varpi,t)$ is the drift, $h(\varpi,t)$ is the diffusion and dB_t is the differential for the random process typically taken as the Weiner process. (Note that the above SDE can then be readily adapted to a

particle-based numerical method where each particle represents a stochastic realization). Furthermore, any random function, $G(\varpi,t)$ that is twice differentiable is expanded using stochastic calculus:

$$dG(\varpi,t) = \left[\frac{\partial G}{\partial t} + g_t(\varpi,t)\frac{\partial}{\partial \varpi}f(\varpi,t) + \frac{h^2}{2}\frac{\partial^2}{\partial \varpi^2}f(\varpi,t)\right]dt + h(\varpi,t)\frac{\partial}{\partial x_t}f(\varpi,t)dB_t. \quad (2.1.5)$$

This is also known as Ito's Lemma. As noted above, equation 2.1.4 and 2.1.5 are readily adapted to a particle-based numerical method.

The first stochastic modeling approach uses a particle-based numerical method to solve the SDE. The drift portion is a standard Ordinary Differential Equation (ODE) and a diffusion model is arbitrarily chosen. To calibrate the diffusion model, two methods may be used. The first method is based upon repeat experiments, where a mean and variance of the random variable are determined from data. Using the distribution of results from the analyses, the diffusion model may be calibrated. A second approach is to propose a micromechanical or mesomechanical model to characterize random features in the model. The mean and variance of the random feature determines and characterizes the diffusion model of the random variable. The challenge of the first modeling method is using a sufficient number of particles in each computational cell to ensure there is a reasonable and statistically significant distribution. Adaptive particle insertion and deletion have been added to help overcome this difficulty and will be discussed in a following section in this chapter.

The second stochastic modeling approach is based on having reasonable knowledge of how the random variable behaves. This knowledge may be based on experimental observation, micromechanical or mesomechanical analysis, etc. Prescribing a given PDF also determines the moments of the PDF in terms of the drift and diffusion (non-stationary) and preserves the distribution during a given analysis. To do this, we use the forward/reverse Kolmogorov techniques to derive the drift and diffusion models for a given PDF [9]. The details of this stochastic method are discussed in chapter four.

The last modeling approach is based upon the coupling of multiple random variables, called a Joint Probability Density Function (JPDF). This technique does not currently use a particle method to solve the SDEs'. In this stochastic modeling approach, we have several random variables and a model to couple them, called a copula. If multiple independent random variables are used, stochastic modeling approach two is an appropriate solution method. This method is the least general of the three and to date the JPDF is dependent on the PDFs and the random variables making the JPDF application dependent.

2.2. Stochastic Particle Method

To solve the stochastic partial differential equations, a particle method is used. The particle method is a Lagrangian technique and is designed to minimize memory use and be robust. As mentioned in the previous section, methods one and two use the particle method to solve the SDE. The stochastic process is assumed to be the Weiner process (i.e. Brownian motion). In equation 2.1.3, the dB_t term is replaced with a random variable model [14] and the equation is integrated explicitly as,

$$\varpi^{n+1} = \varpi^n + g_t\Delta t + h\xi\sqrt{\Delta t}, \quad (2.2.1)$$

where ϖ^n is the random variable at scaled time n, ϖ^{n+1} is the random variable at time n+1, ξ is random number, (0→1) generated by a uniform random number generator and Δt is the change in

time. The random variable is updated on each particle in the computational cell. After the random variable solution is applied to every particle in a computational cell a binning process is performed by separating the particles into bins. The bin extents of maximum and minimum are found by searching through the particle list in the cell. The bin size is determined by subdividing the range of the minimum and maximum values of the random variable on the particle field. For example, the range of the random variable on the particles are a minimum of 0 (X_0) and a maximum of 1 (X_h). Since the random variable spans 0→1 this may be subdivided into 1000 bins and will have a bin size of 0.001. Therefore, a particle is a value of 0.5001 will fall into one bin and a particle with a value of 0.5100 will fall into a different bin. The resulting binning process will generate a histogram based upon the number of particles in a bin and the bin number, refer to Figure 2-1.

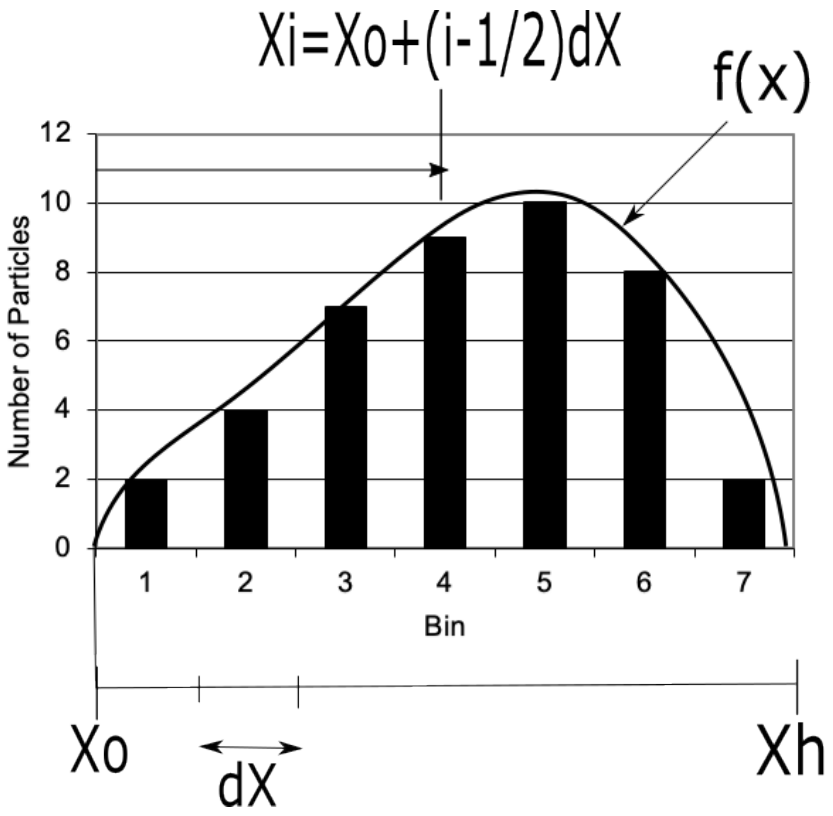

Figure 2-1. Example of particle binning to generate probability density function

There are two horizontal axes in Figure 2-1, one horizontal axis is for the sorting bin number that starts at 0 and ends at the total number of bins (0 to 7 in the above figure). The second horizontal axis is the value of the random variable (X_0 to X_h) field on the particles. Therefore, a normalization process is needed to relate the binning of the particles to physical domain of the random variable defining the PDF, $f(\varpi)$. We start with the following definition:

$$\int_{-\infty}^{\infty} f(\varpi) d\varpi \triangleq 1 \tag{2.2.2}$$

Using Figure 2-1, we represent the above equation numerically,

$$\int_{X_o}^{X_h} f(\varpi)d\varpi \sim \sum_{i=1}^{nb} f(\varpi_i)\Delta\varpi, \tag{2.2.3}$$

and

$$\Delta\varpi = \frac{X_h - X_o}{nb}, \tag{2.2.4}$$

where nb is the number of bins. Next, the distribution function is scaled according to the particle count in each bin, np_i:

$$f(\varpi_i) = \frac{np_i}{scale}. \tag{2.2.5}$$

Using the above equation with Equation 2.2.2 and 2.2.3:

$$\sum_{i=1}^{nb} \frac{np_i}{scale}\Delta\varpi = 1. \tag{2.2.6}$$

Since $\sum_{i=1}^{nb} np_i = npt$, where npt is the total number of particles in the cell, then:

$$f(\varpi_i) = \frac{np_i}{\Delta\varpi\, npt}. \tag{2.2.7}$$

The mean of the PDF is defined as:

$$mean = \mu \triangleq \int_{-\infty}^{\infty} \varpi f(\varpi)d\varpi. \tag{2.2.8}$$

Integrating over the extent of the random variable,

$$\int_{-\infty}^{\infty} \varpi f(\varpi)d\varpi = \int_{X_o}^{X_h} (\varpi - X_o) f(\varpi)d\varpi + X_o, \tag{2.2.9}$$

and numerically,

$$\mu = X_o + \frac{\Delta\varpi}{npt}\sum_{i=1}^{nb}\left(i - \frac{1}{2}\right) * np_i. \tag{2.2.10}$$

The variance of the PDF is defined as:

$$variance = \sigma^2 \triangleq \int_{-\infty}^{\infty} (\varpi - \mu)^2 f(\varpi)d\varpi. \tag{2.2.11}$$

Integrating over the extent of the random variable,

$$\int_{-\infty}^{\infty} (\varpi - \mu)^2 f(\varpi)d\varpi = \int_{X_o}^{X_h} [\varpi - X_o - (\mu - X_o)]^2 f(\varpi)d\varpi, \tag{2.2.12}$$

and numerically,

$$\sigma^2 = \frac{1}{npt}\sum_{i=1}^{nb}\left[\left(i - \frac{1}{2}\right)\Delta\varpi - \hat{\mu}\right]^2 * np_i, \tag{2.2.13}$$

where

$$\hat{\mu} = \frac{\Delta\varpi}{npt}\sum_{i=1}^{nb}\left(i - \frac{1}{2}\right) * np_i. \tag{2.2.14}$$

Lastly, the mean and variance are used to map the random variable from the particles to the grid. This is performed using the following equation,

$$\langle g \rangle = \int_{-\infty}^{\infty} g(\varpi) f(\varpi) d\varpi, \tag{2.2.15}$$

where $g(\varpi)$ is an arbitrary function that is dependent on the random variable ϖ and $f(\varpi)$ is a PDF describing the distribution of the random variable on the grid. The mean and variance from equations 2.2.4 and 2.2.5 are used to compute coefficients of a prescribed PDF. As an example, the Normal or Gaussian PDF uses the mean and variance directly,

$$f(\varpi) = \frac{1}{\sigma\sqrt{2\pi}} e\left[-\frac{(\varpi - \mu)^2}{2\sigma^2}\right]. \tag{2.2.16}$$

Performing the integration in Equation 2.2.6, the mean quantity $\langle g \rangle$ is determined on the computational grid.

2.3. Particle Motion

In this section, the particle motion will be highlighted. Previous work on particle methods has been performed in [15]; and for this work, only the motion of the particle is used. The position of the particle is updated using the following equation,

$$\boldsymbol{pos}^{n+1} = \boldsymbol{pos}^{n} + \boldsymbol{v}^{p}\Delta\tau, \tag{2.4.1}$$

where $\boldsymbol{v}^{p}$ is the velocity vector interpolated to the particle from the computational grid and $\Delta\tau$ is the current timestep. In the case of the velocities located on the face, the velocities are linearly interpolated to the particle, Figure 2.2. In the case of the velocities located at the vertex, the velocities are linearly interpolated for one-dimensional problems; refer to Figure 2-3. Note: bilinear and trilinear interpolation methods are used for two-dimensional and three-dimension problems, respectively.

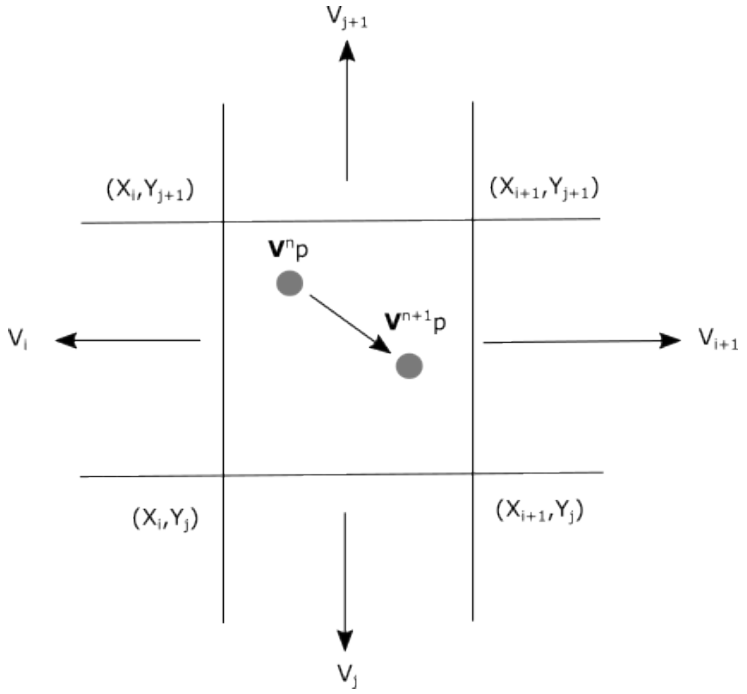

Figure 2-2. Particle face velocity interpolation and position update

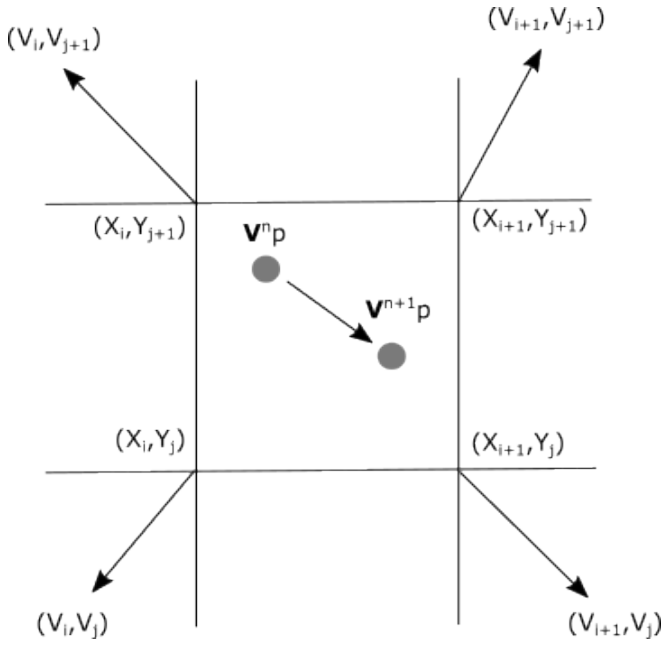

Figure 2-3. Particle vertex velocity interpolation and position update

.

2.4. Adaptive Particle Insertion and Deletion

In this section, an adaptive particle insertion or deletion process is described. This adaptive process is implemented to control the number of particles during the analysis where computational domains maybe large or where regions of interest do not have enough particles to properly form the particle distribution described above. In the event of a low particle count in a computation cell, the PDF moments cannot generate a mean and variance state with statistical relevance. In contrast, in the event of high particle counts in an area that are not of interest, the particles may be removed. Overall, the adaptive technique, add particles where they are needed and removes particles where they are not needed.

This process mirrors the adaptive mesh refinement (AMR) technique that is used in MC [16]. As was done in AMR, splitting and combining of a block is performed using indicators. Here the indicators communicate the insertion and deletion of the particles in the computational domain. The particles are inserted into the computational cell with the mean value of the cell at the current timestep. The position of particle is randomized using the following equation,

$$\boldsymbol{pos} = \boldsymbol{pos}^0 + \xi_i \Delta \boldsymbol{cell\_size}, \tag{2.4.1}$$

where $\boldsymbol{pos}$ is the particle position vector, $\boldsymbol{pos}^0$ is the cell lowest global position vector, ξ_i is a random number ($0 < \xi < 1$) by grid axis direction and $\Delta\boldsymbol{cell\_size}$ is the cell size vector (length, width, and height). Lastly, when particles are introduced (or removed) into the computational cell, the PDF is preserved.

This page intentionally left blank

3. STOCHASTIC PARTICLE METHOD USING ARBITRARY DIFFUSION

The first of three stochastic modeling approaches that was added to the shock physics code Multiple Component (MC) is a particle based numerical method that uses an arbitrary diffusion model. The stochastic particle method is used to solve a Stochastic Differential Equation (SDE) and the primary distinction between this method and the other methods is the arbitrary nature of the diffusion model. This diffusion model is not specific to a given Probability Density Function (PDF). This stochastic modeling approach is used to determine the PDF that describes the behavior of the random variable.

3.1. Description

This stochastic modeling approach explicitly integrates equation 2.1.3 and is given as equation 2.2.1 on each particle. The drift portion is a standard Ordinary Differential Equation (ODE) and the diffusion model is arbitrarily chosen. A diffusion model that has been previously assumed for various applications [8] is given by,

$$h = k_1 e^{k_2 t}, \tag{3.1.1}$$

where, k_1 and k_2 are model coefficients and t is the current scaled time. There are several choices for diffusion models and this model has a broad range of applicability. If $k_2 = 0$ then the diffusion model is a constant. If additional models are required, they may be added to the computational code as necessary. An existing database of models and their calibration coefficients may be used.

3.2. Example: Stochastic Damage

The failure and damage of materials is of great interest in modeling statistical fracture. The fracture of materials is predominately dictated by the microstructure of the material. Fracture can occur from an accumulation of nucleation sites that eventually coalesce leading to a macroscopic crack. The microstructural damage is generated from several physical phenomena occurring at a level that one cannot measure such as crystal debonding, crystal fracture, etc. These microstructural effects dominate the macroscopic result, and thus stochastic methods are used to model the random generation of damage sites that coalesce into macroscopic failure.

There are several fracture models given in the literature, and a rate dependent damage model is considered here, i.e., the kinetic theory of fracture [17],

$$\frac{d\mathbb{D}}{dt} = \frac{(\mathbb{D}_0 - \mathbb{D})}{\tau_0} e^{\left[\frac{-(U-\gamma S)}{kTA}\right]}, \tag{3.2.1}$$

where $\mathbb{D}$ is damage, $\mathbb{D}_0$ = 1.58, τ_0 is a time constant of 1e-13 seconds, S is stress, k is Boltzmann's constant (1.380649e-16 erg/K), T is temperature, A is Avogadro's number, U and γ are calibration coefficients. Using equations 2.2.1, 3.1.1 and 3.2.1 we arrive at the following SDE,

$$\mathbb{D}_t^{n+1} = \mathbb{D}_t^n + \frac{(\mathbb{D}_{t0} - \mathbb{D}_t^n)}{\tau_0} e^{\left[\frac{-(U-\gamma S)}{kTA}\right]} \Delta t + k_1 e^{k_2 t} \xi \sqrt{\Delta t}. \tag{3.2.2}$$

As outlined in chapter two, the above equation is solved on the particles and the collection of particles is binned to determine the mean damage and variance in the computational cell.

A Weibull distribution is assumed to represent the overall distribution of the random fracture in the cell [2]. First, the Weibull coefficients are given in terms of the mean and variance,

$$f(\mathbb{D}) = \frac{k_w}{\lambda_w}\left(\frac{\mathbb{D}}{\lambda_w}\right)^{k_w-1} e^{-\left[\frac{\mathbb{D}}{\lambda_w}\right]^{k_w}}, \tag{3.2.3}$$

where k_w and λ_w are Weibull calibration coefficients. The Weibull coefficient k_w is computed using an iterative process whereby the left-hand side of the equation is known and the values of gamma are equated to the right-hand side,

$$\frac{\sigma^2}{\mu^2} + 1 = \frac{\frac{2}{k_w}\Gamma\left(\frac{2}{k_w}\right)}{\left[\frac{1}{k_w}\Gamma\left(\frac{1}{k_w}\right)\right]^2}. \tag{3.2.4}$$

where σ^2 is the variance. Once k_w is known, λ_w may be determined,

$$\lambda_w = \frac{\mu}{\frac{1}{k_w}\Gamma\left(\frac{1}{k_w}\right)}. \tag{3.2.5}$$

This calibrated Weibull distribution is used to determine the mean state of the fracture stress F in the cell. Here we use equation 2.2.6,

$$\langle F \rangle = \int_0^1 \frac{k_w}{\lambda_w}\left(\frac{\mathbb{D}}{\lambda_w}\right)^{k_w-1} e^{-\left[\frac{\mathbb{D}}{\lambda_w}\right]^{k_w}} F(1-\mathbb{D})d\mathbb{D}. \tag{3.2.6}$$

where $\langle F \rangle$ is the mean fracture stress. The mean fracture stress is used in the fracture algorithm for inserting material or void, reducing the internal stress and numerically depicting the occurrence of failure.

3.3. Result

To demonstrate the use of this stochastic modeling method, a symmetric impact analysis of copper on copper is performed in one-dimension. The intent of the analysis is to investigate the spall behavior of the copper where microstructure defects may affect the spall strength, time, and location of the spall fracture. To induce spall fracture, two pieces of copper are used where one is an impactor traveling at 210 m/s and the other is a target. The target is twice the length of the impactor; therefore, the spall fracture should occur near the center of the target, L= 1 mm. A graphical description of the analysis problem is shown in Figure, 3-1. The constitutive material model is the Mie-Gruneisen model for the Equation of State, elastic-plastic assuming no hardening and a yield strength value of 25 MPa and the failure model is as described above with an initial spall of 3.5 GPa.

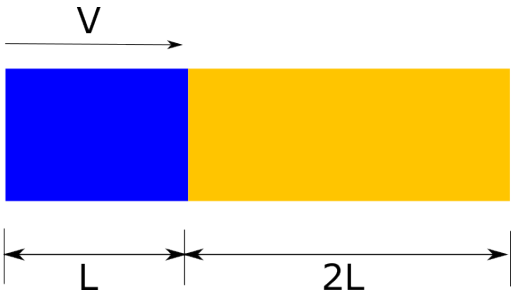

Figure 3-1. Symmetric copper-copper impact

In each cell, a minimum of 100 particles is set to model the stochastic spall behavior. A statistical sample size of 100 was chosen to be of significant size to capture the stochastic spall behavior, therefore 100 analyses have been performed. The spall fracture was determined when the mean fracture stress was exceeded by the material stress. At this point, the analysis was ended, and the time, location and mean fracture stress were recorded. The resulting mean fracture stress is shown in Figure 3-2.

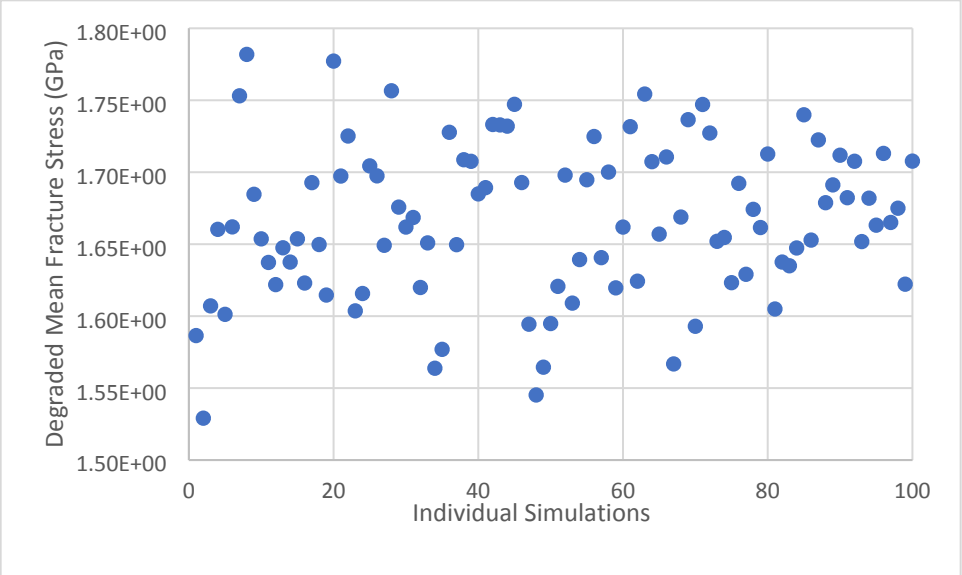

Figure 3-2. Mean fracture stress for symmetric copper-copper impact.

The average fracture stress is 1.67 GPa at fracture and a deviation of 5.28 MPa. The resulting fracture location is shown in Figure 3-3

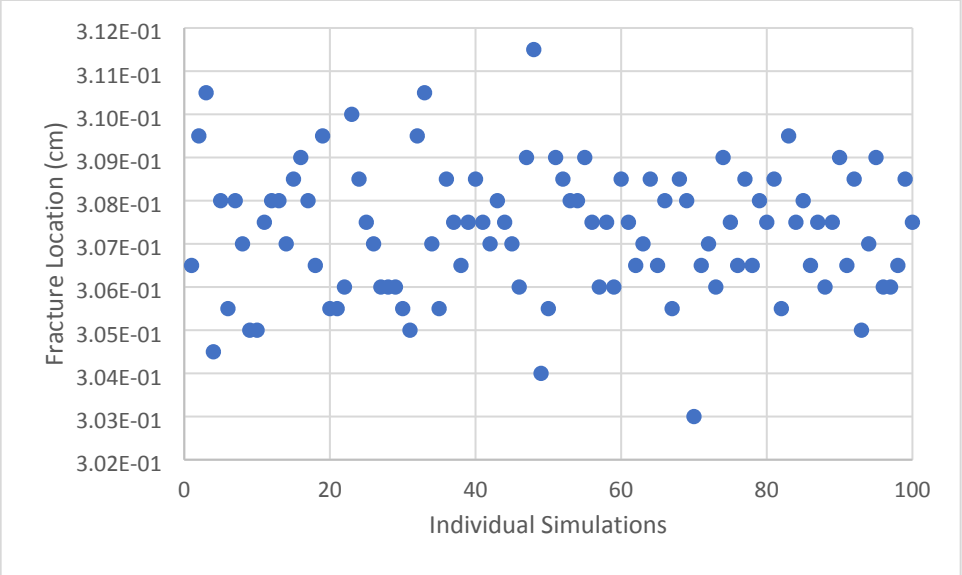

Figure 3-3. Fracture location for symmetric copper-copper impact.

The front of the target is initially located at 0.2 mm. The average fracture location is at 0.307 cm with a deviation of 0.00148 cm. The resulting fracture time is shown in Figure 3-4.

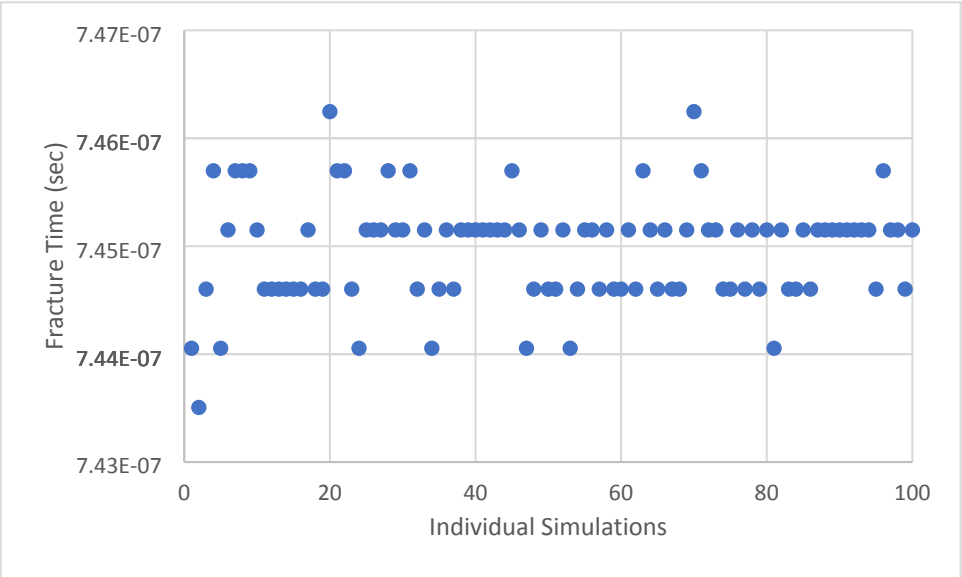

Figure 3-4. Fracture time for symmetric copper-copper impact

The average fracture time is 7.45e-7 seconds and the deviation is 4.85e-10 seconds. The fracture time is shown to be "banded" as the timestep is based upon the Currant-limited timestep. Therefore, the spall fracture occurred within 6 cycles of each other for all 100 analyses.

The variation in the mean fracture stress, time and location are modeled by the diffusion model and its calibration coefficients. For the above analyses, one diffusion model and calibration coefficients were used. With the addition of extra data, the calibration model and coefficients may be refined. In addition, the confirmation of the Weibull PDF may also be performed. Ultimately, the results show the stochastic modeling approach is providing a reasonable result given the assumptions and

calibration coefficients. Assuming this material characterization is correct, the copper material model maybe added to larger system analysis where the copper material used.

This page intentionally left blank

4. STOCHASTIC PARTICLE METHOD BASED UPON FORWARD/BACKWARD KOLMOGOROV METHODS

This chapter highlights the second stochastic approach developed and implemented into the computational shock physics code MC. Once again, this method uses the stochastic particle method to describe the material stochastic behavior. The primary difference in this approach is that the diffusion and drift models are based upon the Probability Density Function (PDF) through the forward and backward Kolmogorov equations.

This stochastic modeling method preserves the form of the PDF fit to the random variable using defined drift and diffusion models. The drift and diffusion models are defined based upon the PDF and the forward/backward Kolmogorov equations. Using this stochastic modeling approach there are two different types of Kolmogorov results, stationary and non-stationary. A non-stationary Kolmogorov result provides the drift and diffusion models of the PDF that evolve in time. In contrast, the stationary Kolmogorov result provides the drift and diffusion models of the PDF fixed (stationary) in time. Additional equations are needed to describe the evolution of the mean and variance quantities. To help understand this process, we first start with a description of the forward/backward Kolmogorov approach with models implemented into MC and finally an application with results.

4.1. Forward/Backward Kolmogorov with Stochastic Models of Drift and Diffusion

The forward Kolmogorov approach has been well documented in literature [9]. Starting with Equation 2.1.1,

$$d\varpi = g_t(\varpi,t)dt + h(\varpi,t)dB_t \tag{4.1.1}$$

where g_t is a drift function, h is a diffusion function, ϖ is the random variable and t is scaled time. Now, we introduce the forward/backward Kolmogorov equations as,

$$\frac{\partial f(\varpi,t)}{\partial t} + \frac{\partial (g(\varpi,t)f(\varpi,t))}{\partial \varpi} - \frac{1}{2}\frac{\partial^2 \left(h(\varpi,t)^2 f(\varpi,t)\right)}{\partial \varpi^2} = 0 \tag{4.1.2}$$

$$\frac{\partial f(\varsigma,s)}{\partial s} + g(\varsigma,s)\frac{\partial f(\varsigma,s)}{\partial \varsigma} + \frac{1}{2}h(\varsigma,s)^2\frac{\partial^2 f(\varsigma,s)}{\partial \varsigma^2} = 0 \tag{4.1.3}$$

The first equation, 4.1.2, is the forward Kolmogorov equation based in independent variables ϖ and t. The second equation, 4.1.3, is the backward Kolmogorov equation based in independent variables ς and s. The change in $\varpi - \varsigma$ occurs over the timestep, $t - s$. Using these two equations and a given distribution function f, equations for g and h are derived as functions of forward variables only, ϖ and t. A strongly stationary designation requires the mean and variance do not vary with time. The weakly stationary designation defines the mean and variance will vary with time. The functions g and h are provided below for a few given PDFs'.

4.1.1. Normal/Gaussian

$$f(\varpi,t) = \frac{1}{\sqrt{2\pi}\sigma} e^{-\frac{1}{2}\left[\frac{\varpi-\mu}{\sigma}\right]^2} \tag{4.1.4}$$

$$g(\varpi,t) = \frac{1}{2}[\varpi - \mu] + \frac{\partial \mu}{\partial t} \tag{4.1.5}$$

$$h^2(\varpi,t) = \sigma^2 + \frac{\partial \sigma^2}{\partial t} \tag{4.1.6}$$

4.1.2. Weibull

$$f(\varpi,t) = \frac{k_w}{\lambda_w}\left[\frac{\varpi - m_w}{\lambda_w}\right]^{k_w - 1} e^{-\left(\frac{\varpi - m_w)}{\lambda_w}\right)^{k_w}} \tag{4.1.7}$$

$$g(\varpi,t) = [\varpi - m_w] + [\varpi - m_w]^{1-k_w}\left[\frac{{\lambda_w}^{k_w}}{k_w} + \frac{\frac{\partial {\lambda_w}^{k_w}}{\partial t}}{{k_w}^2}\right] + \frac{\partial m_w}{\partial t} \tag{4.1.8}$$

$$h^2(\varpi,t) = 2[\varpi - m_w]^{2-k_w}\left[\frac{{\lambda_w}^{k_w}}{k_w} + \frac{\frac{\partial {\lambda_w}^{k_w}}{\partial t}}{{k_w}^2}\right] \tag{4.1.9}$$

4.1.3. Frechet

$$f(\varpi,t) = \frac{\alpha_F}{s_F}\left[\frac{\varpi - m_F}{s_F}\right]^{-1-\alpha_F} e^{-\left(\frac{\varpi - m_F)}{s_F}\right)^{-\alpha_F}} \tag{4.1.10}$$

$$g(x,t) = [\varpi - m_F] + [\varpi - m_F]^{1+\alpha_F}\left[\frac{s^{-\alpha_F}}{\alpha_F} + \frac{\frac{\partial s^{-\alpha_F}}{\partial t}}{{\alpha_F}^2}\right] + \frac{\partial m_F}{\partial t} \tag{4.1.11}$$

$$h^2(\varpi,t) = 2[\varpi - m_F]^{2+\alpha_F}\left[\frac{s^{-\alpha_F}}{\alpha_F} + \frac{\frac{\partial s^{-\alpha_F}}{\partial t}}{{\alpha_F}^2}\right] \tag{4.1.12}$$

4.1.4. Generalized Extremum

$$f(\varpi,t) = \frac{1}{s_E}\left[1 + \alpha_E\left(\frac{\varpi - m_E}{s_E}\right)\right]^{-1-\frac{1}{\alpha_E}} e^{-\left[1+\alpha_E\left(\frac{\varpi - m_E}{s_E}\right)\right]^{-\frac{1}{\alpha_E}}} \tag{4.1.13}$$

$$g(\varpi,t) = s_E + \alpha_E(\varpi - m_E) + \alpha_E s_E^{-\frac{1}{\alpha_E}}[s_E + \alpha_E(\varpi - m_E)]^{1+\frac{1}{\alpha_E}} +$$

$$\left\{\alpha_E[s_E+\alpha_E(\varpi-m_E)]^{1+\frac{1}{\alpha_E}}+{s_E}^{1+\frac{1}{\alpha_E}}\right\}\left(\frac{\partial {s_E}^{-\frac{1}{\alpha_E}}}{\partial t}\right)+\frac{\partial m_E}{\partial t} \tag{4.1.14}$$

$$h^2(\varpi,t)=2[s_E+\alpha_E(\varpi-m_E)]^{2+\frac{1}{\alpha_E}}\left[{s_E}^{-\frac{1}{\alpha_E}}+\frac{\partial {s_E}^{-\frac{1}{\alpha_E}}}{\partial t}\right] \tag{4.1.15}$$

4.2. Example: Stochastic Reactive Flow

This example is built upon previous work performed by Baer et. al. [1] and Baer [18], where a stochastic ignition model has been previously developed. The purpose of the model is to macroscopically capture the ignition process that occurs within the microstructure using stochastics. We start with the first law of thermodynamics applied at the microstructure level to capture the hotspot phenomena and the coalescence of the hotspots to generate ignition; these equations are presented below as,

$$\frac{\partial\langle T\rangle}{\partial t}=\alpha\nabla^2\langle T\rangle+\int_0^\infty\frac{\Delta H_{rel}}{\langle C_p\rangle}Ae^{-\frac{E_a}{R\zeta}}f(\zeta)d\zeta, \tag{4.2.1}$$

and

$$\frac{\partial\langle\sigma_T^2\rangle}{\partial t}=\alpha\nabla^2\sigma_T^2+2C_1-2C_2\sigma_T^2+\int_0^\infty\frac{\Delta H_R}{\langle C_p\rangle}Ae^{-\frac{E_a}{R\zeta}}2(\zeta-\langle T\rangle)f(\zeta)d\zeta, \tag{4.2.2}$$

where T is the solid temperature (random variable), α is the material thermal diffusivity, C_p is the specific heat capacity, ΔH_{rel} is the heat release by reaction, R is the gas constant, A and E_a are calibration coefficients and C_1 and C_2 are diffusion model calibration coefficients. In the above references, the distribution was assumed to be Gaussian and here we present the distribution as the Fréchet PDF. This PDF has been chosen based upon the results of mesoscale analysis where the Fréchet distribution shows a better agreement to energetic ignition processes. The integrations are performed using the Laplace expansion method resulting in the following for the integration in Equation 4.2.1,

$$\int_0^\infty\frac{\Delta H_R}{\langle C_p\rangle}Ae^{-\frac{E_a}{R\zeta}}f(\zeta)d\zeta=\sqrt{\frac{2\pi}{M|\phi''(x_0)|}}h(x_0)e^{(M\phi(x_0))} \tag{4.2.3}$$

$$x_0=\frac{1}{(1+P)^2} \tag{4.2.4}$$

$$M=\left(\frac{E_a}{s_FR\alpha_F}\right)^{\frac{\alpha_F}{\alpha_F+1}} \tag{4.2.5}$$

$$P=\frac{m_F}{s_F}\left(\frac{E_a}{s_FR\alpha_F}\right)^{\frac{-1}{\alpha_F+1}} \tag{4.2.6}$$

$$\phi(x_0)=\frac{-\alpha_F}{\frac{1}{x_0^{\alpha_F}}+P}-x_0 \tag{4.2.7}$$

$$\phi''(x_0) = \frac{P(\alpha_F - 1)x_0^{\frac{1}{\alpha_F}-2} + (\alpha_F + 1)x_0^{\frac{2}{\alpha_F}-2}}{\alpha_F\left(P + x_0^{\frac{1}{\alpha_F}}\right)^3} \tag{4.2.8}$$

$$h(x_0) = AM\frac{\Delta H_R}{\langle C_p \rangle} \tag{4.2.9}$$

Where α_F is the PDF calibration parameter, not to be confused with α as the thermal diffusivity. The integration of the integral in equation 4.2.2 is shown below,

$$\int_0^\infty \frac{\Delta H_R}{\langle C_p \rangle} Ae^{-\frac{E_a}{R\zeta}} 2(\zeta - \langle T \rangle) f(\zeta) d\zeta = \sqrt{\frac{2\pi}{M|\phi''(x_0)|}} h(x_0) e^{(M\phi(x_0))} \tag{4.2.10}$$

$$x_0 = \frac{1}{(1+P)^2} \tag{4.2.11}$$

$$M = \left(\frac{E_a}{s_F R \alpha_F}\right)^{\frac{\alpha_F}{\alpha_F + 1}} \tag{4.2.12}$$

$$P = \frac{m_F}{s_F}\left(\frac{E_a}{s_F R \alpha_F}\right)^{\frac{-1}{\alpha_F + 1}} \tag{4.2.13}$$

$$\phi(x_0) = \frac{-\alpha_F}{x_0^{\frac{1}{\alpha_F}} + P} - x_0 \tag{4.2.14}$$

$$\phi''(x_0) = \frac{P(\alpha_F - 1)x_0^{\frac{1}{\alpha_F}-2} + (\alpha_F + 1)x_0^{\frac{2}{\alpha_F}-2}}{\alpha_F\left(P + x_0^{\frac{1}{\alpha_F}}\right)^3} \tag{4.2.15}$$

$$h(x_0) = 2A\frac{\Delta H_R}{\langle C_p \rangle}\left(m_F + x_0 s_F M^{\frac{1}{\alpha_F}} - \langle T \rangle\right) \tag{4.2.16}$$

The mean and variance equations 4.2.1 and 4.2.2 provide the non-stationary equations needed to complete the Fréchet stochastic equation of 4.1.1. Using the mathematical relationship of the mean and variance,

$$\langle T \rangle = m_F + s_F \Gamma\left(1 - \frac{1}{\alpha_F}\right) \tag{4.2.17}$$

$$\langle \sigma_T^2 \rangle = {s_F}^2\left\{\Gamma\left(1 - \frac{2}{\alpha_F}\right) - \left[\Gamma\left(1 - \frac{1}{\alpha_F}\right)\right]^2\right\} \tag{4.2.18}$$

We take the non-dimensional time derivate on these functions,

$$\frac{\partial m_F}{\partial t} = \frac{\partial \langle T \rangle}{\partial t} - \frac{\partial s_F}{\partial t}\Gamma\left(1 - \frac{1}{\alpha_F}\right) - s_F\frac{\partial}{\partial t}\Gamma\left(1 - \frac{1}{\alpha_F}\right) \tag{4.2.19}$$

$$\frac{\partial {s_F}^2}{\partial t} = \left\{ \frac{1}{\Gamma\left(1-\frac{1}{\alpha_F}\right) - \left[\Gamma\left(1-\frac{2}{\alpha_F}\right)\right]^2} \right\} \left\{ \frac{\partial \langle \sigma_T^2 \rangle}{\partial t} - s_F \frac{\partial}{\partial t} \left[\Gamma\left(1-\frac{2}{\alpha_F}\right) - \left[\Gamma\left(1-\frac{1}{\alpha_F}\right)\right]^2 \right] \right\} \tag{4.2.20}$$

These equations are solved on each particle just as in stochastic modeling method one. The particles are binned according to the solid temperature and new mean and variance values are computed. From the mean and variance, the new s_F, m_F and α_F values are computed for the Fréchet PDF.

4.3. Result

To demonstrate the use of this stochastic modeling approach, we will be modeling a piston compaction experiment consisting of Bullseye gunpowder in one-dimension, Figure 4.1. Bullseye gunpowder composition is (60% NC-13, 40 % NG) and the density used in this study is 0.68 g/cc (tap density where solid volume fraction is 41.5%). Previous work has been performed to calibrate a reactive flow model from experimental data (see Schumacher and Baer [19]), where the calibration is deterministic however, energetic materials are known to be non-deterministic near the threshold of ignition. In this case, the piston compresses the distended Bullseye to near full dense and the material ultimately reacts. Here we will use the stochastic reactive flow model as described above.

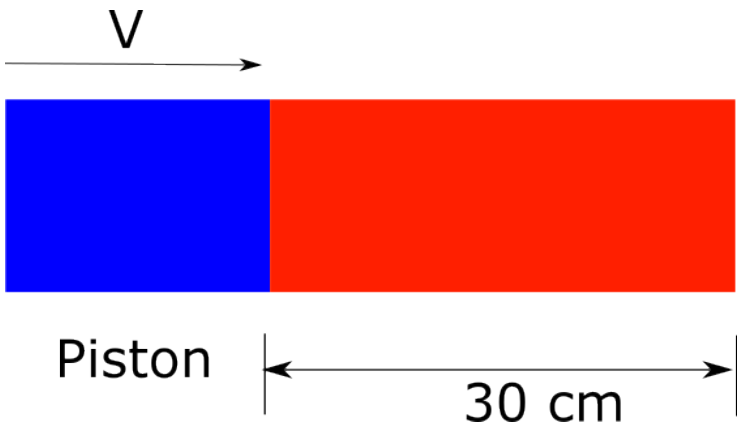

Figure 4-1. Piston impact of distended energetic material

We first start with a PDF that is assumed to be the Fréchet PDF as motivated by mesoscale modeling [20]. The Fréchet distribution is initialized so the first moment is set to the mean room temperature, Figure 4-2. The particle field is initialized using a randomization of the mean state using the second moment and random variables. Therefore, the mean state of the temperature in a computation cell is the mean room temperature and the binning process of the particle field replicates the initial PDF.

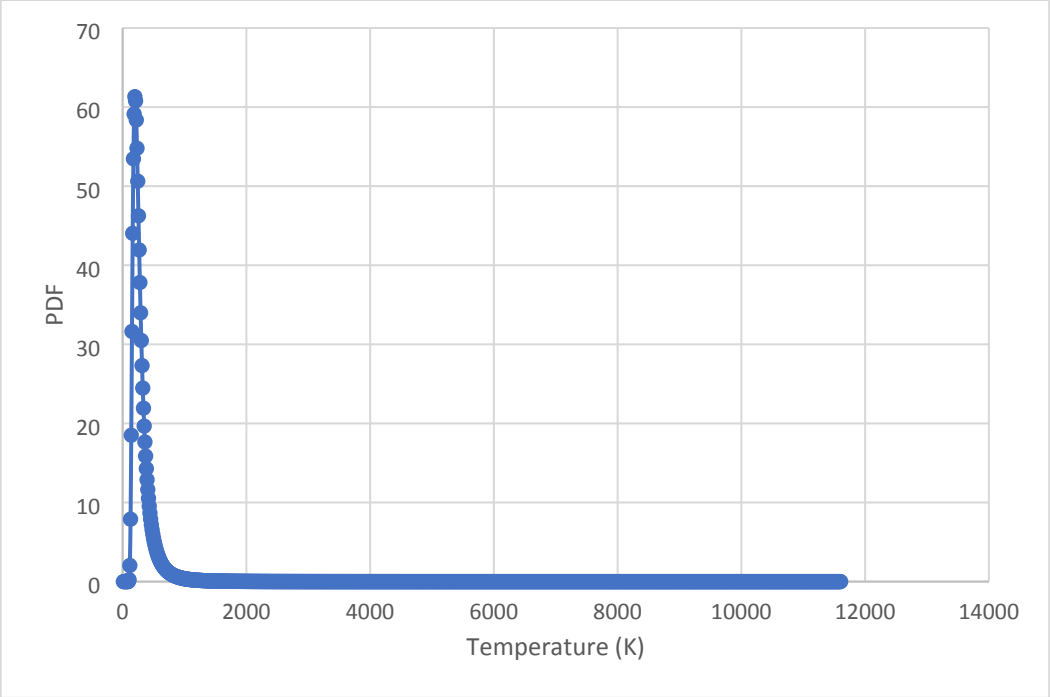

Figure 4-2. Fréchet probability density function initial state.

Once the particles have been initialized the simulation proceeds using Equations 4.1.1, 4.1.11 and 4.1.12 to compute the solid temperature on each particle. The particle field is therefore binned and the new first moment, μ_n, and second moment, ${\sigma_n}^2$, are computed. From these moments the updated Fréchet PDF constants s_F and m_F are computed with a constant α_F.

$$s_F = \sqrt{\frac{{\sigma_n}^2}{\left(1-\frac{2}{\alpha_F}\right)-\left[\Gamma\left(1-\frac{1}{\alpha_F}\right)\right]^2}} \tag{4.3.1}$$

$$m_F^n = \mu_n - s_F\Gamma\left(1-\frac{1}{\alpha_F}\right) \tag{4.3.2}$$

A statistical sample size of 100 realizations were chosen to capture the stochastic ignition of the Bullseye material, therefore 100 analyses have been performed. The ignition of the energetic was assumed when the product gas exceeded a temperature of approximately 4000 K. This temperature was chosen because it is approximately the Chapman-Jouguet temperature, 4061 K, for reacted Bullseye when the reactive wave travels at the detonation velocity. At this ignition point the ignition temperature, time and location were recorded. The resulting mean gas temperature is shown in Figure 4-3.

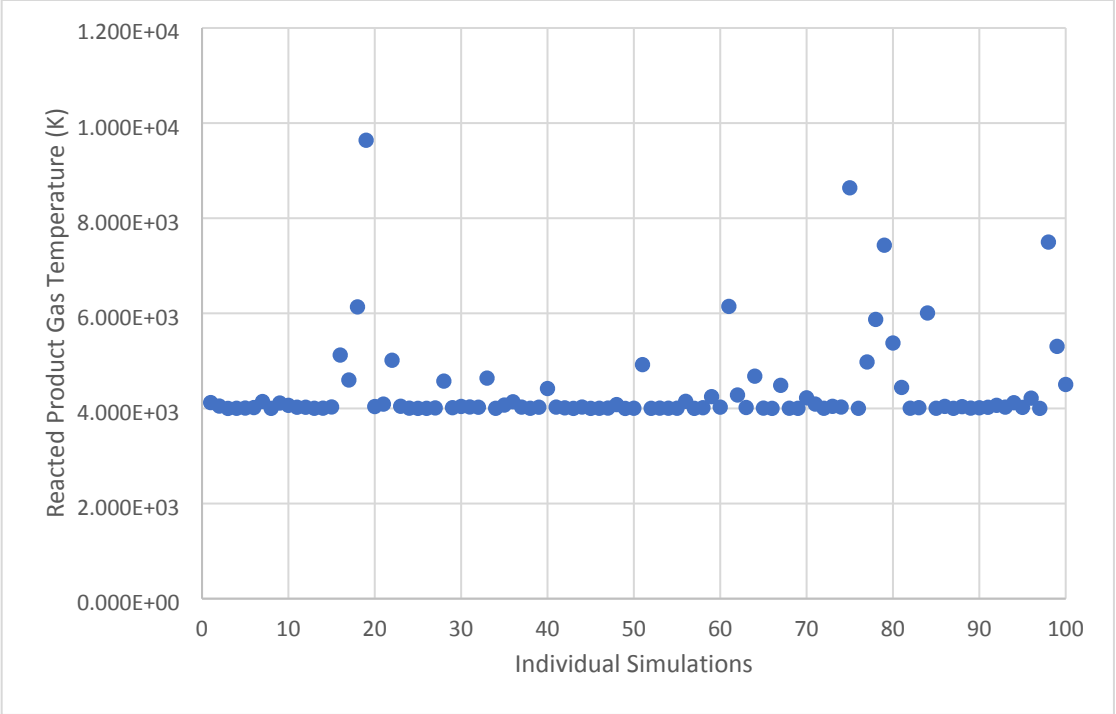

Figure 4-3. Gas Temperature at ignition of Bullseye with piston velocity at 150 m/s.

The mean gas temperature is 4395 K at ignition and a deviation of 942 K. The resulting ignition time is shown in Figure 4-4.

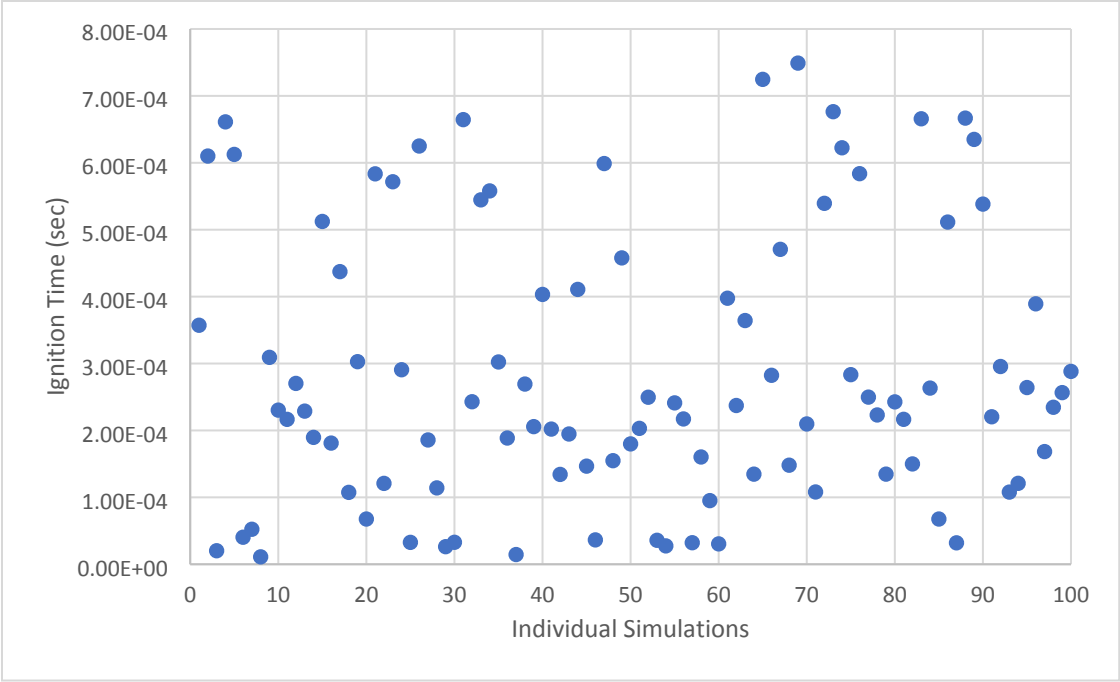

Figure 4-4. Ignition time of Bullseye with piston velocity at 150 m/s

The average ignition time is 2.87e-4 seconds and the deviation is 2.03e-4 seconds. The resulting ignition location is shown in Figure 4-5.

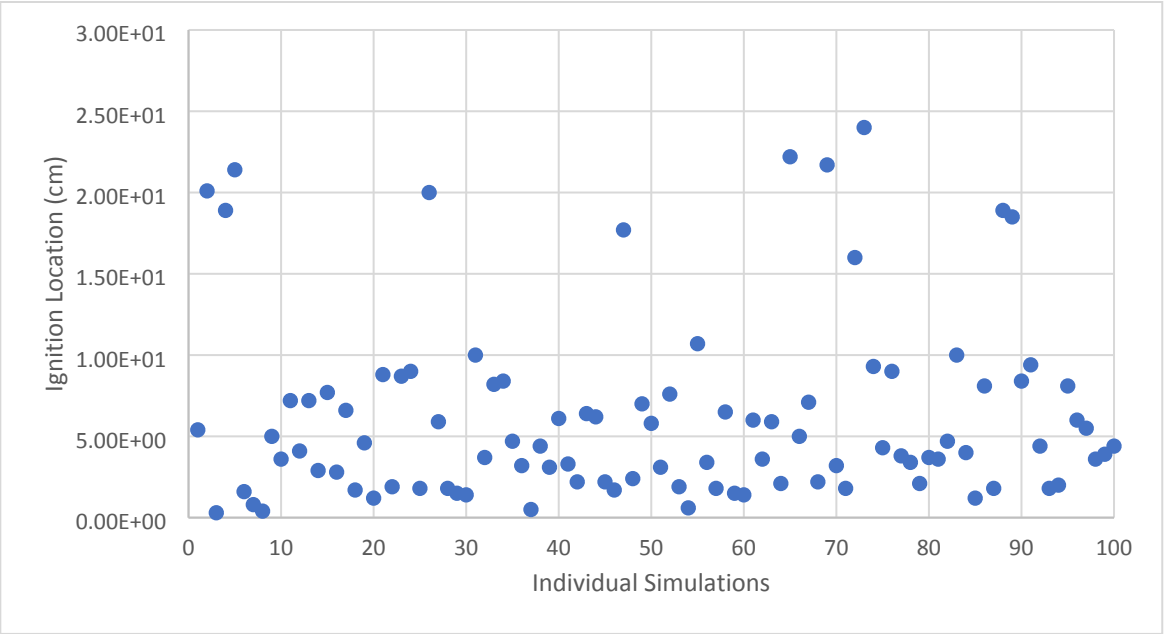

Figure 4-5. Ignition location of Bullseye with piston velocity at 150 m/s

The initial location front of the Bullseye is at 0 cm. The average ignition location is at 6.15 cm with a deviation of 5.57 cm.

The results demonstrate the use of stochastic modeling technique using the forward/backward Kolmogorov approach. As mentioned above, the technique includes the effect of the microstructure to describe the mean and variance evolution of the PDF. The reaction rate is controlled using a single step chemical kinetic equation with the Fréchet PDF. These moments determine the stochastic nature of the energetic ignition process. The influence of the chosen Fréchet PDF is readily seen in Figures 4-4 and 4-5 with the noticeable banding at the bottom of the figures and tails in the upper portion of the Figures.

Additional analysis cases have been omitted from the above figures because the product gas did not meet or exceed 4000K. However, several instances of the product gas ranged between 2000K – 3999K. In these cases, the reactive wave was traveling at 1500 m/s to 2000 m/s. The reaction was not entirely supported by the detonation state, but the reaction wave is traveling fast enough that the net outcome of a test would be labeled "violent" or "significant reaction".

5. STOCHASTIC MODELING METHOD FOR JOINT PROBABILITY DENSITY FUNCTIONS

The last stochastic modeling approach is the union of multiple random variables. This is performed by joining multiple single random processes using a copula which is a multivariant Cumulative Distribution Function (CDF) or Joint Cumulative Distribution Function (JCDF). A copula function describes the interdependence of the random variables. For the special case of a bivariant, two random variables of ϖ and ς,

$$JCDF(\varpi,\varsigma) = F(\varpi,\varsigma) = \left(\mu_{\varpi},\mu_{\varsigma},\sigma_{\varpi}^2,\sigma_{\varsigma}^2,F(\varpi),F(\varsigma)\right), \tag{5.0.1}$$

where, μ_{ϖ} and μ_{ς} are the means, σ_{ϖ}^2 and σ_{ς}^2 are the variances, and $F(\varpi)$ and $F(\varsigma)$ are the CDFs for random variables ϖ and ς, respectively. The marginal CDFs are computed using the following,

$$F_{\varpi}(\varpi) \triangleq \lim_{\varsigma\to\infty} F(\varpi,\varsigma) \quad for\ any\ \varpi\ , \tag{5.0.2}$$

$$F_{\varsigma}(\varsigma) \triangleq \lim_{\varpi\to\infty} F(\varpi,\varsigma) \quad for\ any\ \varsigma\ , \tag{5.0.3}$$

also,

$$F(\infty,\infty) = 1\ , \tag{5.0.4}$$

$$F(-\infty,\varsigma) = 0\ , \tag{5.0.5}$$

and

$$F(\varpi,-\infty) = 0\ . \tag{5.0.6}$$

The bivariant Joint Probability Distribution Function (JPDF) is defined from the bivariant CDF as,

$$f(\varpi,\varsigma) \triangleq \frac{\partial\text{^}2F(\varpi,\varsigma)}{\partial\varpi\partial\varsigma}. \tag{5.0.7}$$

A general relationship for a bivariant JPDF is,

$$\int_{-\infty}^{\infty}\int_{-\infty}^{\infty} f(\varpi,\varsigma)d\varpi d\varsigma \triangleq 1\ . \tag{5.0.8}$$

The marginal computation for a bivariant JPDF with random variables is ϖ and ς:

$$f_{\varpi}(\varpi) \triangleq \int_{-\infty}^{\infty} f(\varpi,\varsigma)d\varsigma\ , \tag{5.0.9}$$

and

$$f_{\varsigma}(\varsigma) \triangleq \int_{-\infty}^{\infty} f(\varpi,\varsigma)d\varpi\ , \tag{5.0.10}$$

where $f_{\varpi}(\varpi)$ and $f_{\varsigma}(\varsigma)$ are the marginal PDFs for random variables ϖ and ς, respectively. In addition, the CDF and PDF are related by the following definitions,

$$f_{\varpi}(\varpi) \triangleq \frac{\partial F_{\varpi}(\varpi)}{\partial \varpi}, \tag{5.0.11}$$

and

$$f_{\varsigma}(\varsigma) \triangleq \frac{\partial F_{\varsigma}(\varsigma)}{\partial \varsigma}. \tag{5.0.12}$$

The mean and variance of the random variable ϖ is shown below where the mean and variance of the random variable, ς, is similar,

$$\mu_{\varpi} \triangleq \int_{-\infty}^{\infty} \varpi f_{\varpi}(\varpi) d\varpi \tag{5.0.13}$$

$$\sigma_{\varpi}^2 \triangleq \int_{-\infty}^{\infty} (\varpi - \mu_{\varpi})^2 f_{\varpi}(\varpi) d\varpi \tag{5.0.14}$$

The covariance is computed as,

$$\sigma_{\varpi\varsigma}^2 \triangleq \int_{-\infty}^{\infty} \int_{-\infty}^{\infty} (\varpi - \mu_{\varpi})(\varsigma - \mu_{\varsigma}) f(\varpi,\varsigma) d\varpi d\varsigma, \tag{5.0.15}$$

or

$$\sigma_{\varpi\varsigma}^2 = \int_{-\infty}^{\infty} \int_{-\infty}^{\infty} \varpi\varsigma f(\varpi,\varsigma) d\varpi d\varsigma - \mu_{\varpi}\mu_{\varsigma}, \tag{5.0.16}$$

where $\sigma_{\varpi\varsigma}^2$ is the covariance. A measure of the interdependence of the random variables ϖ and ς is described by the correlation coefficient. The classical coefficient of correlation as,

$$corr \triangleq \frac{\sigma_{\varpi\varsigma}^2}{\sqrt{\sigma_{\varpi}^2 \sigma_{\varsigma}^2}}. \tag{5.0.17}$$

Typical values range from -1 (strong negative relationship) to +1(strong positive relationship). In the case of a strong positive relationship, if random variable ϖ increases, then ς will increase also. In the case of a strong negative relationship, if random variable ϖ decreases, then ς will increase.

5.1. Copula

There are several forms of copula functions available to couple PDFs. Insight into the random variable interdependency is useful, however it is difficult to determine. Using techniques such as mesoscale modeling may help provide insight into the coupling of the variables. For the purpose of this work, we present the following copula function from Gumbel [10,11] (also known as the Farlie-Gumble-Morgenstern (FGM) copula),

$$F(\varpi,\varsigma) = F(\varpi)F(\varsigma)\{1 + \vartheta[(1 - F(\varpi))(1 - F(\varsigma))]\} \tag{5.1.1}$$

where $F(\varpi,\varsigma)$ is the bivariant CDF of random variables ϖ and ς, $F(\varpi)$ is the CDF of random variable ϖ, $F(\varsigma)$ is the CDF for random variable ς and ϑ is a coupling coefficient, $(-1 < \vartheta < 1)$. Computing the marginals of the JCDF using Equations 5.0.2 and 5.0.3 we arrive at,

$$F_{\varpi}(\varpi) = F(\varpi) = \lim_{\varsigma \to \infty} F(\varpi,\varsigma), \tag{5.1.2}$$

and

$$F_{\varsigma}(\varsigma) = F(\varsigma) = \lim_{\varpi \to \infty} F(\varpi,\varsigma)\ , \tag{5.1.3}$$

where

$$\lim_{\varpi \to \infty} F(\varpi) = 1\ , \tag{5.1.4}$$

and

$$\lim_{\varsigma \to \infty} F(\varsigma) = 1\ . \tag{5.1.5}$$

To obtain the Joint Probability Density Function (JPDF) we use Equation 5.0.7 and 5.1.1. Expanding Equation 5.1.1 and taking the first derivative in x, we derive,

$$F(\varpi,\varsigma) = F(\varpi)F(\varsigma) + \vartheta F(\varpi)F(\varsigma) - \vartheta F(\varpi)^2 F(\varsigma) - \vartheta F(\varpi)F(\varsigma)^2 + \vartheta F(\varpi)^2 F(\varsigma)^2, \tag{5.1.6}$$

and

$$\frac{\partial F(\varpi,\varsigma)}{\partial \varpi} = f(\varpi)F(\varsigma) + \vartheta f(\varpi)F(\varsigma) - \vartheta 2F(\varpi)f(\varpi)F(\varsigma) - \vartheta f(\varpi)F(\varsigma)^2 + \vartheta 2F(\varpi)f(\varpi)F(\varsigma)^2. \tag{5.1.7}$$

Lastly, taking the second derivative in ς and collecting terms,

$$\frac{\partial F(\varpi,\varsigma)}{\partial \varpi \partial \varsigma} = f(\varpi,\varsigma) = f(\varpi)f(\varsigma)\{1 + \vartheta[(2F(\varpi) - 1)(2F(\varsigma) - 1)]\}. \tag{5.1.8}$$

The marginals of Equation 5.1.8 are computed using Equations 5.0.9 and 5.0.10 resulting in the following,

$$f_{\varpi}(\varpi) = f(\varpi) = \int_{-\infty}^{\infty} f(\varpi,\varsigma)d\varsigma, \tag{5.1.9}$$

and

$$f_{\varsigma}(\varsigma) = f(\varsigma) = \int_{-\infty}^{\infty} f(\varpi,\varsigma)d\varpi. \tag{5.1.10}$$

5.2. Example: Stochastic Reactive Flow with Damage

The modeling of damaged energetics has been performed in several forms in the past. Here we present another path for modeling damaged energetic materials in the aspect of energetic ignition. One of the challenges is to define what damage physically represents since direct measurements of damage do not currently exist. Here, we will define damage as the creation of additional surface area within the energetic without causing volume changes. This is a similar modeling approach developed at SNL with the resulting model called the DaMaGe Induced Reaction model (DMGIR) [20]. Experiments were performed where energetics ignited under given loadings producing ignition that is not sufficiently modeled using our classic Standard Detonation Transition (SDT) pressure-based modeling techniques. In the previous modeling approach, damage is modeling the increase in surface area, that does not produce a volume change. Other definitions of damage include the concept of increased surface area with the increase in porosity, and here we will consider the porosity as a separate physical process that is not considered a damaged process. Specific damage processes are not separated in this analysis, therefore crack formation, decohesion, etc. are all combined as, "damage".

The problem of interest centers on determining when reaction takes place, that defines an "ignition" condition. To define an ignition condition, a model is needed to describe the reaction and the damage "enhanced" reaction behavior. Therefore, we appeal to a stochastic model, specifically, a JPDF is required to couple the reaction and damage to define an averaged mass/energy source as needed for the Multiple Component (MC) computational shock physics code [7]. To describe the reaction behavior, we appeal to a reaction progress random variable, λ, where $0 < \lambda < 1$. A similar process has been performed using the "Ignition and Growth" model [8] and rather than using the "Ignition and Growth" model, an Arrhenius model will be used for this analysis. The reaction progress random variable as,

$$\frac{d\lambda}{dt} = \frac{C_s^+}{\gamma_s}, \tag{5.2.1}$$

where C_s^+ is the mass exchange rate and γ_s is the true density of the condensed (solid) phase. A reasonable approximation of the thermal field at the microstructural level as related to the reaction progress random variable is,

$$T \sim T_0 + \frac{\Delta H_{rel}\lambda}{\gamma_s C_p}, \tag{5.2.2}$$

where T is temperature, T_0 is the initial temperature, ΔH_{rel} is the change in energy due to reaction and C_p is the specific heat at constant pressure. Therefore, the proposed model for the mass exchange rate is given as,

$$\langle C_s^+ \rangle = -\gamma_s \int_0^1 \int_0^1 A e^{\left(\frac{-Ea}{RT}\right)} G(\mathbb{D}) f(\mathbb{D},\lambda) d\mathbb{D} d\lambda, \tag{5.2.3}$$

where $f(\mathbb{D},\lambda)$ is the JPDF as defined in terms of damage random variable, $\mathbb{D}$ $(0 < \mathbb{D} < 1)$, and the reaction progress random variable, λ; also A and E_a are model constants and R is the gas constant. $G(\mathbb{D})$ reflects the change in specific surface area as defined by the damage random variable,

$$G(\mathbb{D}) = 1 + B_{\mathbb{D}} \mathbb{D}^{m_{\mathbb{D}}}, \tag{5.2.4}$$

where $B_{\mathbb{D}}$ and $m_{\mathbb{D}}$ are model constants. From above, the undamaged material is reflected as $G(\mathbb{D}) = 1$ and as $\mathbb{D} \to 1$, the surface area changes increase the mass exchange rate $G(\mathbb{D}) = 1 + B_{\mathbb{D}}$. The model parameter $B_{\mathbb{D}}$ maybe set to $B_{\mathbb{D}} \gg 0$, thus greatly enhancing the reaction process. Similar to the spall fracture problem presented in Chapter 3, we have the evolution of the random damage and reaction progress variables on the particle. The drift function for the damage random variable on the particle is given as (Equation 3.2.1),

$$\frac{d\mathbb{D}}{dt} = \frac{(\mathbb{D}_0 - \mathbb{D})}{\tau_0} e^{\left[\frac{-(U-\gamma S)}{kTA}\right]}, \tag{5.2.5}$$

where T is provided by Equation 5.2.2, $U$and γ are model constants, S is stress, k is Boltzmann's constant, A is Avogadro's number, $\mathbb{D}_0$ = 1.58, τ_0 is a time constant of 1e-13. The reaction progress random variable on the particle is given as,

$$\frac{d\lambda}{dt} = e^{\left(\frac{-Ea}{RT}\right)}. \tag{5.2.6}$$

As was in the case of Chapter 3, a particle method is used to define the moments of the random variables $\mathbb{D}$ and λ. The ordinary differential equations in Equation 5.2.5 and 5.2.6 contain the dependence of both $\mathbb{D}$ and λ. The correct application of the Ito Calculus is to define the Stochastic Differential Equations (SDEs) on a particle where information for $\mathbb{D}$ and λ are carried by the particle. Just as in the case of stochastic spallation in Chapter 3, a diffusion model is assumed. Potentially, meso-scale modeling or representative volume elements can provide insight to these descriptions, however for the purpose of this analysis and exponential function is used, Equation 3.1.1. The explicitly integrated SDE for the damage random variable on the particle is given as,

$$\mathbb{D}^{n+1} = \mathbb{D}^n + \frac{(\mathbb{D}_0 - \mathbb{D}^n)}{\tau_0} e^{\left[\frac{-(U-\gamma S)}{BoltzTA}\right]} \Delta t + k_{\mathbb{D}1} e^{k_{\mathbb{D}2} t} \xi \sqrt{\Delta t}. \tag{5.2.7}$$

where $k_{\mathbb{D}1}$ and $k_{\mathbb{D}2}$ are model coefficients, t is scaled time, Δt is the change scaled time and ξ is random number, (0→1) generated by a random number generator. The explicitly integrated SDE for the reaction progress random variable on the particle is given as,

$$\lambda^{n+1} = \lambda^n + e^{\left(\frac{-Ea}{RT}\right)} \Delta t + k_{\lambda 1} e^{k_{\lambda 2} t} \xi \sqrt{\Delta t}. \tag{5.2.8}$$

where $k_{\lambda 1}$ and $k_{\lambda 2}$ are calibration coefficients.

The JPDF is generated using the copula described above in Section 1, Equation 5.1.6. The CDF for the damage random variable is assumed to be the Weibull as was done in Chapter 3,

$$F(\mathbb{D}) = F_{\mathbb{D}}(\mathbb{D}) = 1 - e^{-\left[\frac{\mathbb{D}}{\lambda_w}\right]^{k_w}}, \tag{5.2.9}$$

and the PDF is,

$$f(\mathbb{D}) = f_{\mathbb{D}}(\mathbb{D}) = \frac{k_w}{\lambda_w}\left(\frac{\mathbb{D}}{\lambda_w}\right)^{k_w - 1} e^{-\left[\frac{\mathbb{D}}{\lambda_w}\right]^{k_w}}. \tag{5.2.10}$$

The CDF for the reaction progress random variable is assumed to be the Fréchet model as was done in Chapter 4,

$$F(\lambda) = F_r(\lambda) = e^{-\left(\frac{\lambda}{s_F}\right)^{-\alpha_F}}, \tag{5.2.11}$$

and the PDF is,

$$f(\lambda) = f_{\lambda}(\lambda) = \frac{\alpha_F}{s_F}\left[\frac{\lambda}{s_F}\right]^{-1-\alpha_F} e^{-\left(\frac{\lambda}{s_F}\right)^{-\alpha_F}}. \tag{5.2.12}$$

Furthermore, the correlation coefficient using the above PDFs for damage and reaction progress is used to solve for the coupling coefficient. The correlation coefficient, $corr$, can be determined using the particle field. Therefore, using the JPDF, Weibull PDF and the Fréchet PDF we can determine

the relationship of the correlation coefficient to the coupling coefficient, ϑ. The variance of the Weibull PDF is computed as,

$$\sigma_{\mathbb{D}}^2 = {\lambda_w}^2\left\{\Gamma\left(1+\frac{2}{k_w}\right)-\left[\Gamma\left(1+\frac{1}{k_w}\right)\right]^2\right\} \tag{5.2.13}$$

and for the Fréchet PDF where $(\alpha_F > 2)$,

$$\sigma_{\lambda}^2 = {s_F}^2\left\{\Gamma\left(1-\frac{2}{\alpha_F}\right)-\left[\Gamma\left(1-\frac{1}{\alpha_F}\right)\right]^2\right\} \tag{5.2.14}$$

Using Equation 5.0.11, we compute the covariance using the JPDF, Weibull PDF and the Fréchet PDF as,

$$\sigma_{\mathbb{D}\lambda}^2 = \vartheta\left\{\mu_{\mathbb{D}}\mu_{\lambda}-\mu_{\lambda}s_F 2^{\frac{1}{\alpha_F}}\Gamma\left(1-\frac{1}{\alpha_F}\right)+\left[\Gamma\left(1+\frac{1}{k_w}\right)\left(2\lambda_w-\frac{\lambda_w}{2^{\frac{1}{k_w}}}\right)\right]\left[\mu_{\lambda}-s_F 2^{1+\frac{1}{\alpha_F}}\Gamma\left(1-\frac{1}{\alpha_F}\right)\right]\right\} \tag{5.2.15}$$

Using Equation 5.0.17, the correlation coefficient (corr) is computed using the particle field. Once the correlation coefficient is computed, the coupling coefficient may be computed by combining Equations, 5.2.13-5.2.15 and Equation 5.0.17 as:

$$\vartheta = \frac{corr\sqrt{{\lambda_w}^2{s_F}^2\left\{\Gamma\left(1+\frac{2}{k_w}\right)-\left[\Gamma\left(1+\frac{1}{k_w}\right)\right]^2\right\}\left\{\Gamma\left(1-\frac{2}{\alpha_F}\right)-\left[\Gamma\left(1-\frac{1}{\alpha_F}\right)\right]^2\right\}}}{\mu_{\mathbb{D}}\mu_{\lambda}-\mu_{\lambda}s_F 2^{\frac{1}{\alpha_F}}\Gamma\left(1-\frac{1}{\alpha_F}\right)+\left[\Gamma\left(1+\frac{1}{k_w}\right)\left(2\lambda_w-\frac{\lambda_w}{2^{\frac{1}{k_w}}}\right)\right]\left[\mu_{\lambda}-s_F 2^{1+\frac{1}{\alpha_F}}\Gamma\left(1-\frac{1}{\alpha_F}\right)\right]}. \tag{5.2.16}$$

5.3. Result

To demonstrate this use of this stochastic modeling approach, we will be modeling a piston impacting a billet of Composition B energetic material (40% TNT and 60% RDX) in one-dimension, Figure 5-1. The impact velocity of the piston is 250 ms/s.

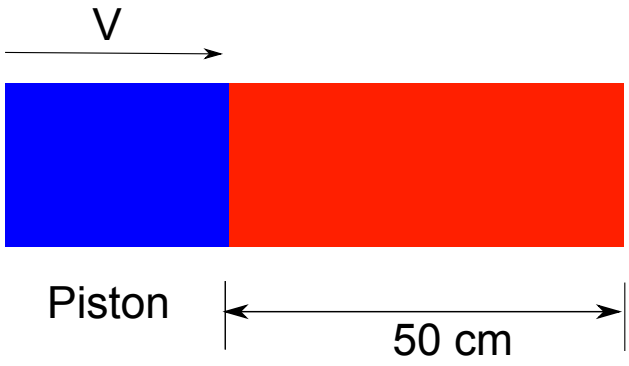

Figure 5-1. Piston impact of Composition B energetic material

For the stochastic ignition process, the Fréchet Probability Density Function (PDF) is chosen, and for the stochastic damage evolution process the Weibull PDF is chosen. The PDF's are coupled using the copula given in Equation 5.1.1 and the initial coupling coefficient is computed from the PDFs initial conditions using Equation 5.2.16. The Fréchet distribution is initialized to a near constant room temperature, Figure 5-2, and the Weibull distribution is initialized to a near 0 damage state of the energetic, Figure 5-3.

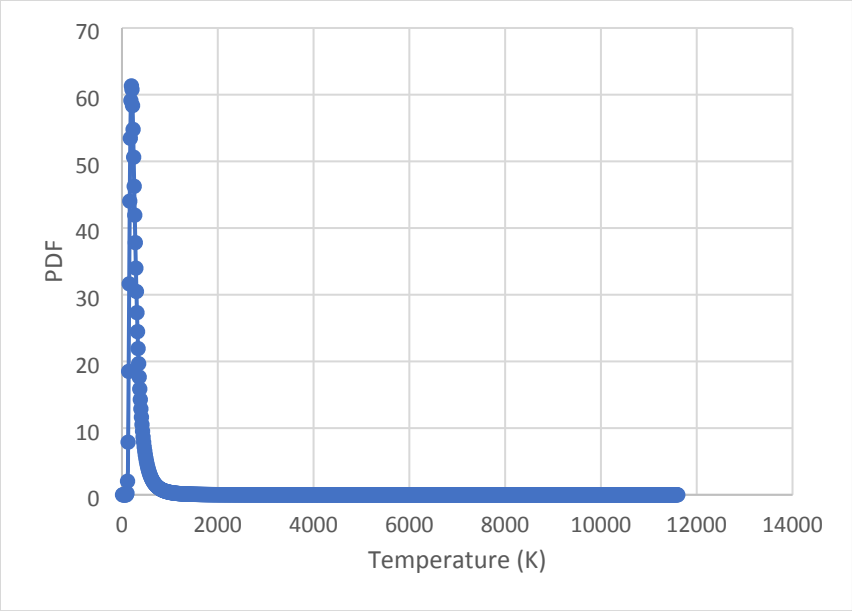

Figure 5-2. Fréchet probability density function initial state.

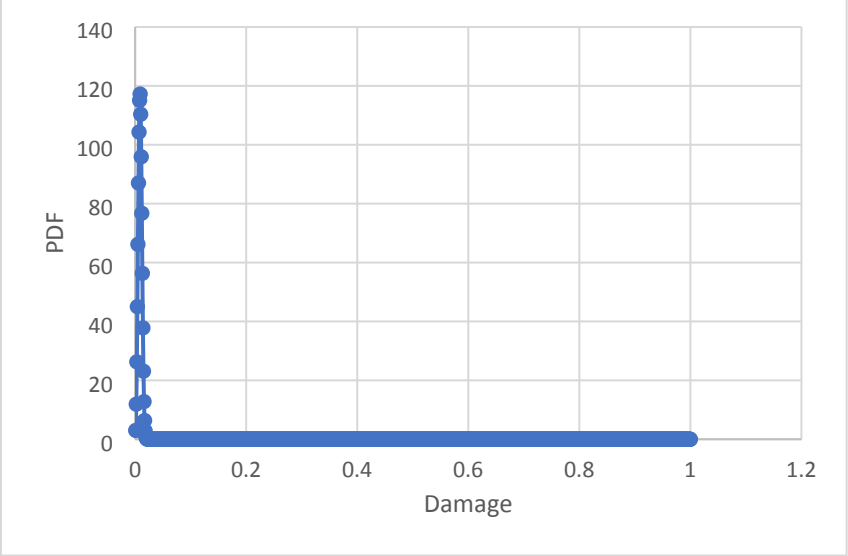

Figure 5-3. Weibull probability density function initial state.

The damage model is calibrated to Hopkinson Bar data generated by Thompson, et al. [21]. This calibration fit is shown below for Composition B in tension and compression, in Figures 5-4 and 5-5. To support this material behavior the damage model was modified to support the tension and

compression failure state of the material. The same Weibull distribution model is assumed in tension and compression. The model coefficients are provided in Table 5-1.

Table 5-1 Kinetic Theory of Fracture parameters for Composition B

	U (erg/mole)	Gamma (1/(dynes/cm^2))
Tension	1.08E5	7300
Compression	1.14E5	7300

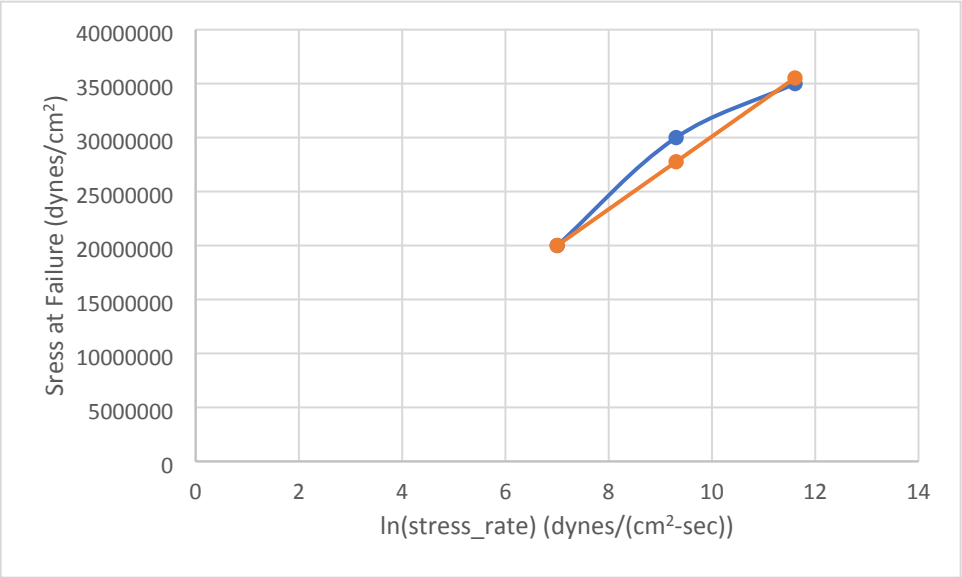

Figure 5-4. Tension failure model calibration (data in blue and the model fit in orange).

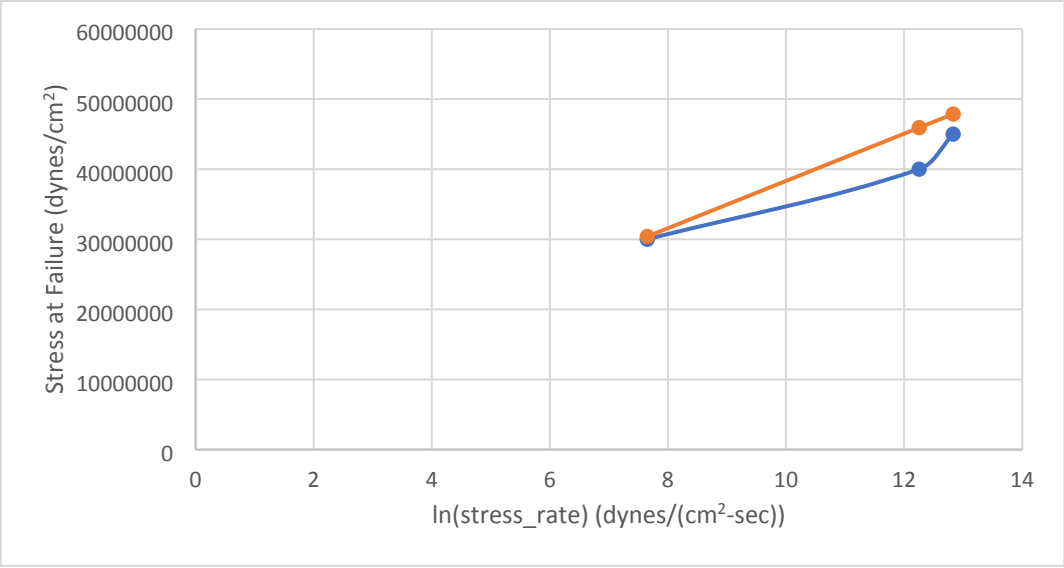

Figure 5-5. Compression failure model calibration (data in blue and the model fit in orange).

A statistical sample size of 100 realizations were chosen to capture the stochastic ignition of the Composition B material, therefore 100 analyses have been performed. The ignition of the energetic was assumed when the product gas exceeded a temperature of approximately 3500 K. This temperature was chosen because it is approximately the Chapman-Jouguet temperature, 3544 K, for reacted Composition B when the reactive wave travels at the detonation velocity. At this ignition point the ignition temperature, time and location were recorded. The resulting mean gas temperature is shown in Figure 5-6.

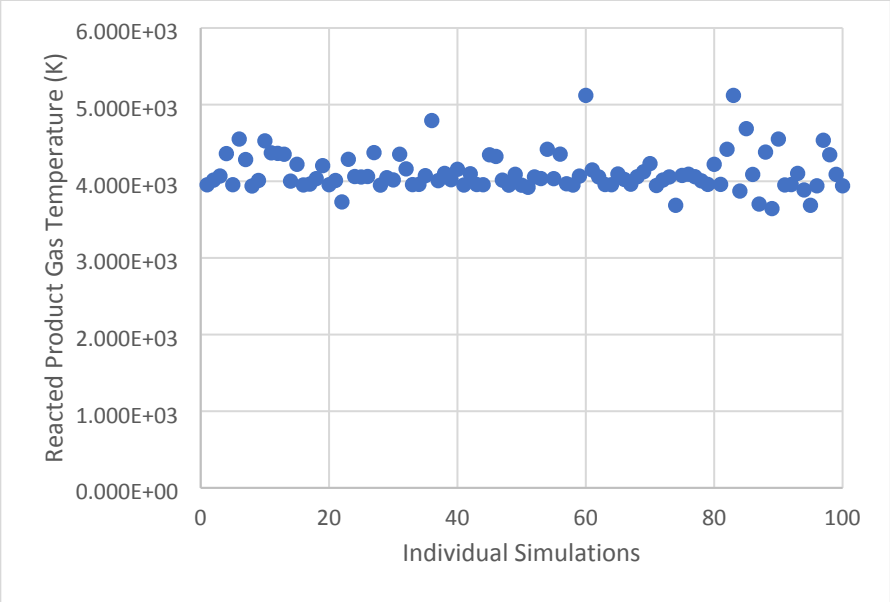

Figure 5-6. Gas Temperature at ignition of Composition B with piston velocity at 250 m/s.

The mean gas temperature is 4114 K at ignition and a deviation of 252 K. The resulting ignition time is shown in Figure 5-7.

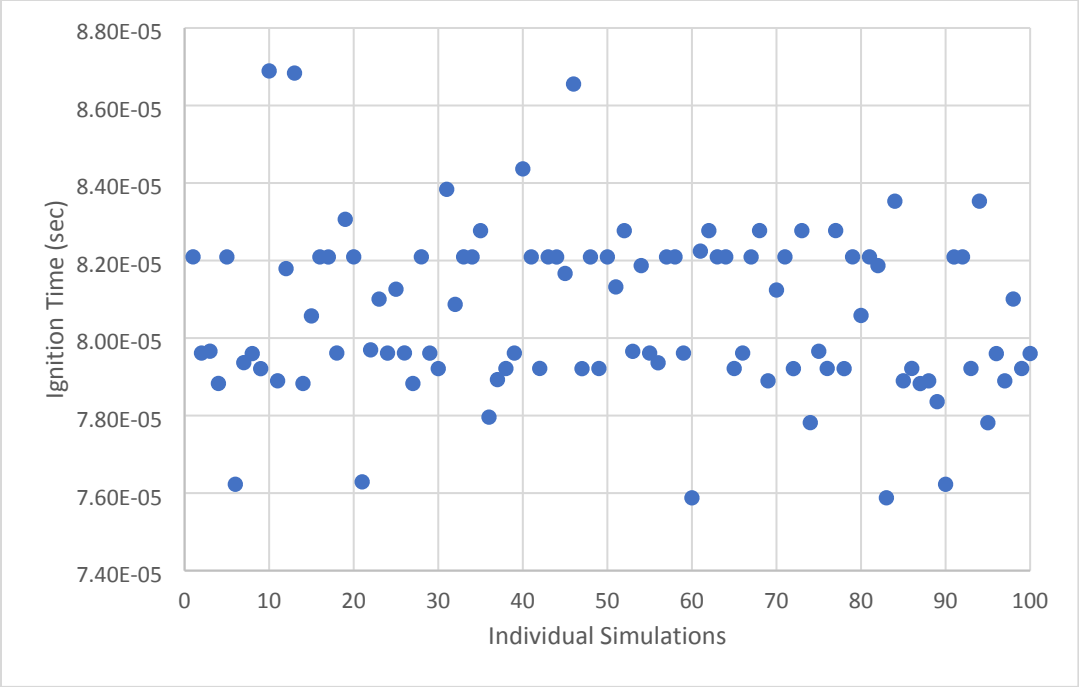

Figure 5-7. Ignition time of Composition B with piston velocity at 250 m/s.

The average ignition time is 8.06e-5 seconds and the deviation is 2.13e-6 seconds. The resulting ignition location is shown in Figure 5-8.

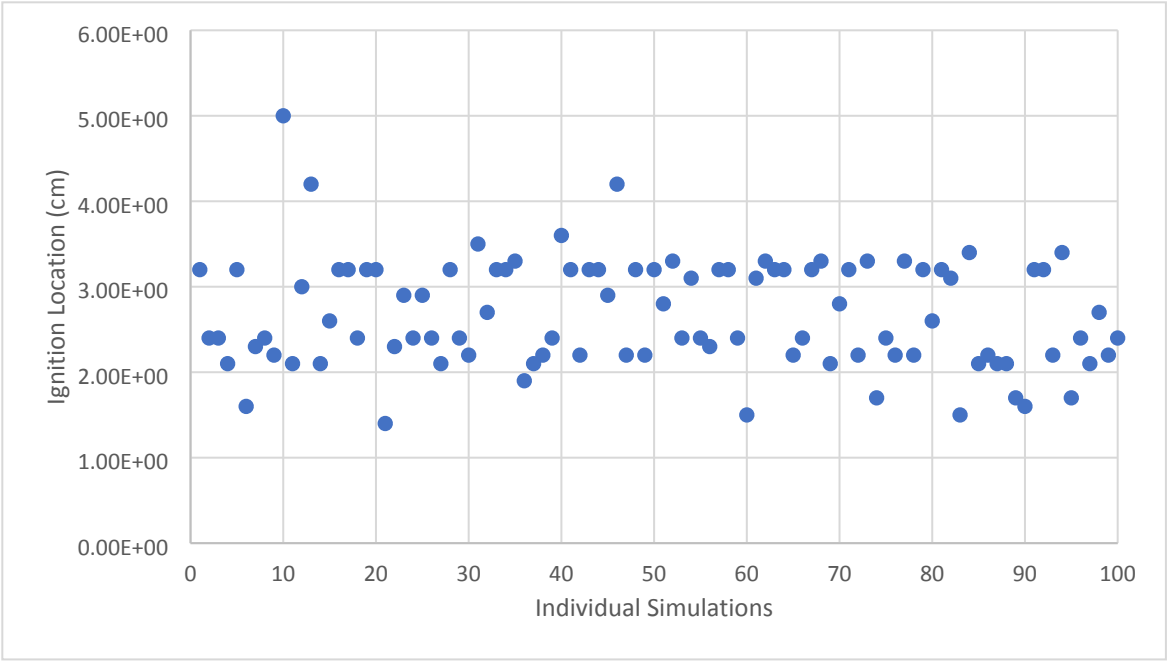

Figure 5-8. Ignition location of Composition B with piston velocity at 250 m/s.

The initial location front of the Composition B is at 0 cm. The average ignition location is 6.15 cm with a deviation of 0.635 cm. The resulting damage state at ignition is shown in Figure 5-9.

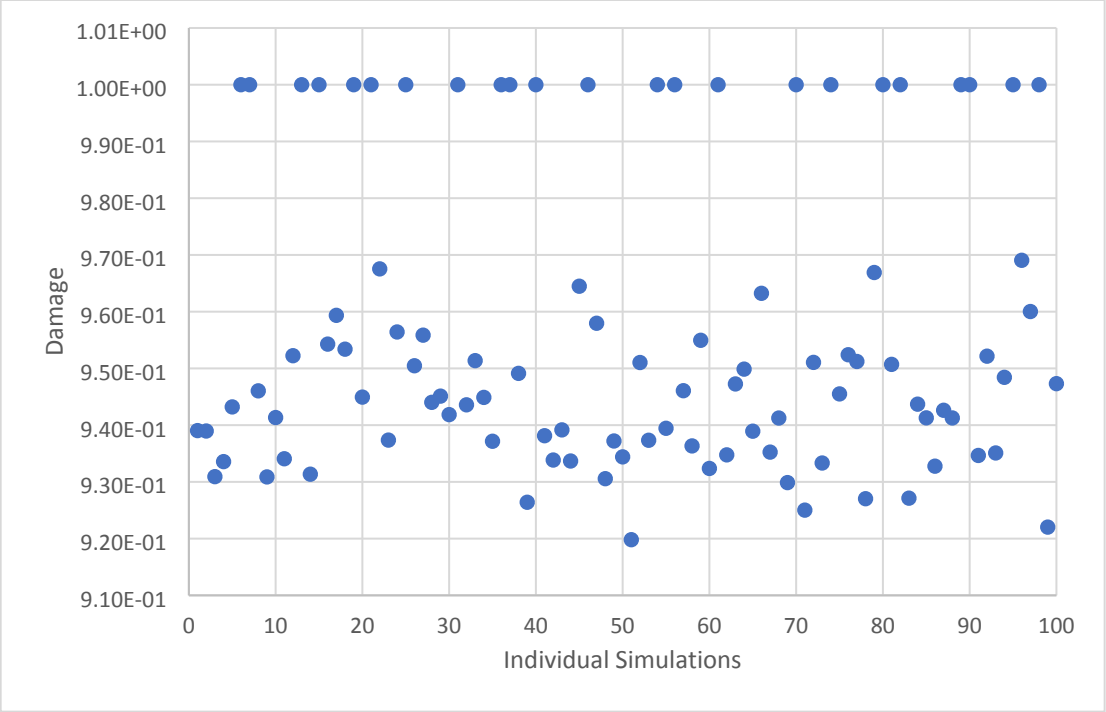

Figure 5-9. Damage state at ignition of Composition B with piston velocity at 250 m/s

The average damage at ignition is 0.96 and the deviation is 0.026.

To further illustrate the use of the coupled damage and reaction model with stochastics, we have recorded the PDF coefficients and the coupling coefficient in Table 5-2. These values are recorded at the ignition point.

Table 5-2 JPDF model coefficients at ignition

Time (s)	k_w	λ_w	α_F	s_F	ϑ
0	3.9	4.60e-9	7.50	3.47e-11	-6.80e-3
60e-6	75.8	0.95	20.2	7.63e-5	-0.12
79.2e-6	46.1	0.95	3.10	0.09	-6.17e-4

The initial (time zero) condition of the energetic material JPDF is plotted in Figure 5-10. The range of the JPDF is $(0 > \mathbb{D} > 1)$ for damage and $(0 > \lambda > 1)$ for the reaction progress. However, at the initial condition, the values are near 0, so the axis ranges have been altered for visualization purposes. The JPDF is plotted at 60e-6 seconds in Figure 5-11 where the data is taken from the computational cell with the highest temperature in the energetic material. The cell data shows the damage is near a value of 1 and the reaction is still near 0. The damage is due to the impact and reaction is seen to start building, but ignition has not occurred. At ignition, time 79.2e-6 seconds for this instance, the resulting JPDF is provided in Figure 5-12. The damage state is approximately the same as at 60e-6 s, however the reaction progress variable has change by ~5 orders of magnitude. The reaction progress variable is ~ 0.12 at ignition. The reaction is enhanced by the damage and for this instance, the reaction is enhanced ~4 times the undamaged material. In Equation 5.2.3, the mass exchange rate includes the coupled damage and rate of reaction. Figure 5-13 is provided to help visualize the JPDF by changing the plot range.

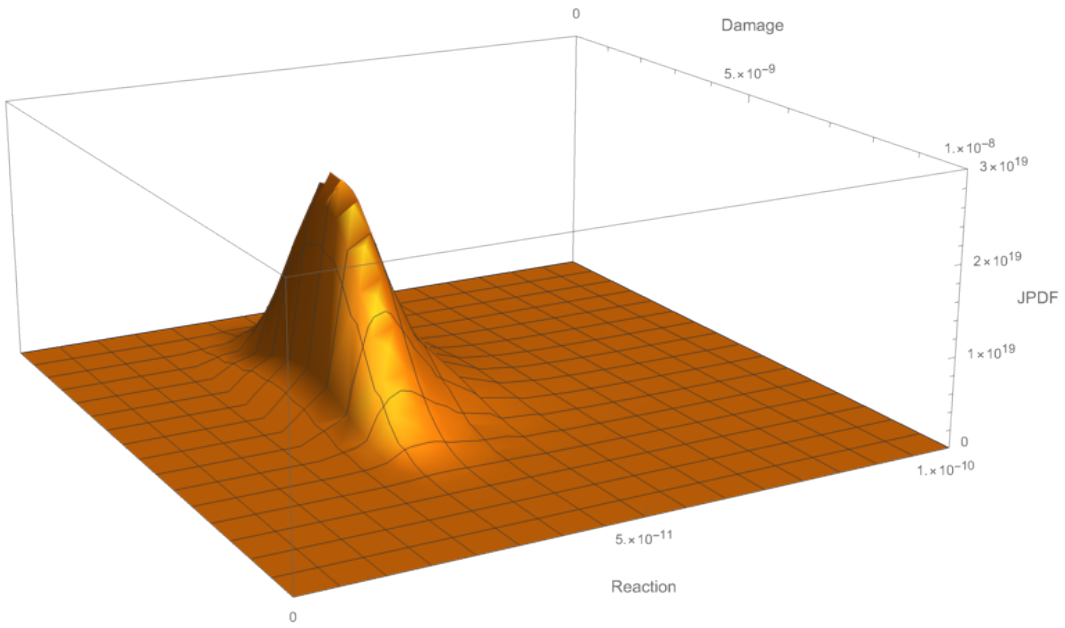

Figure 5-10. initial JPDF for Composition B.

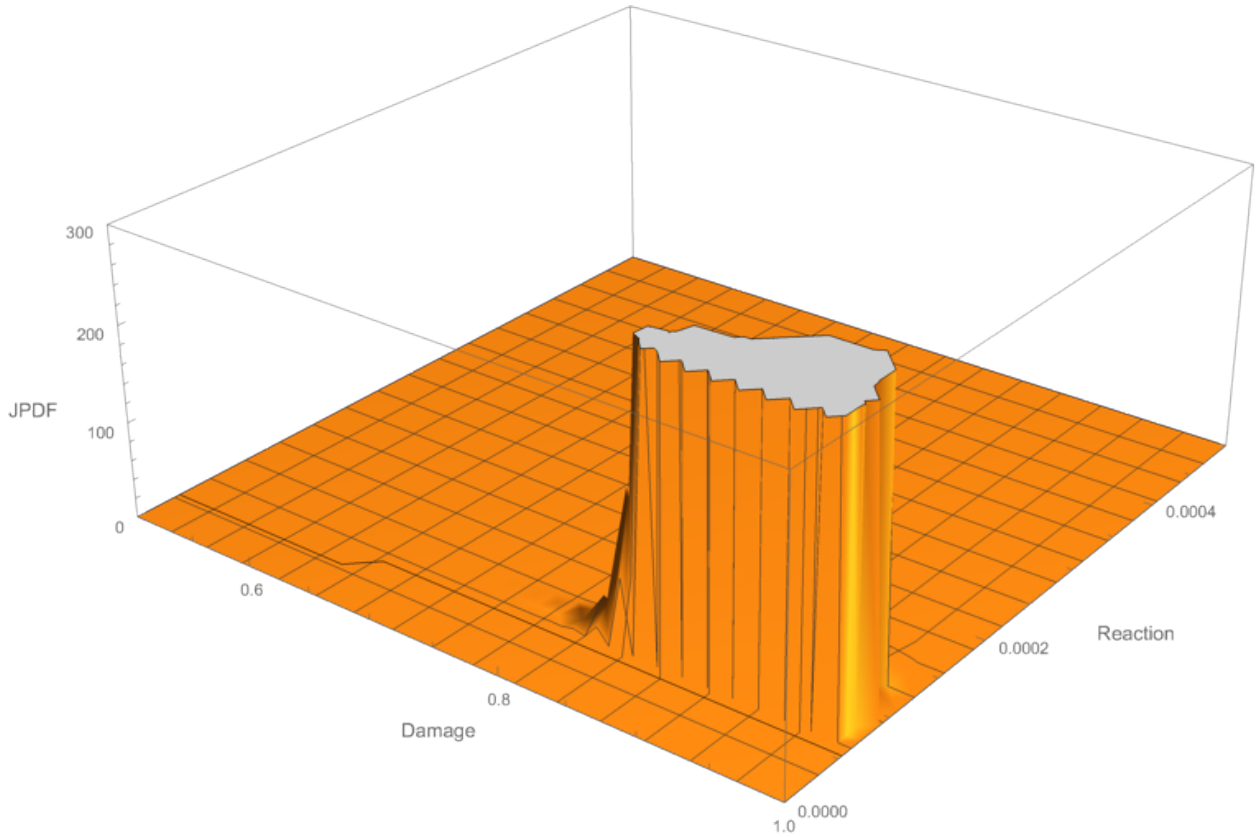

Figure 5-11. JPDF for Composition B at 60e-6 seconds.

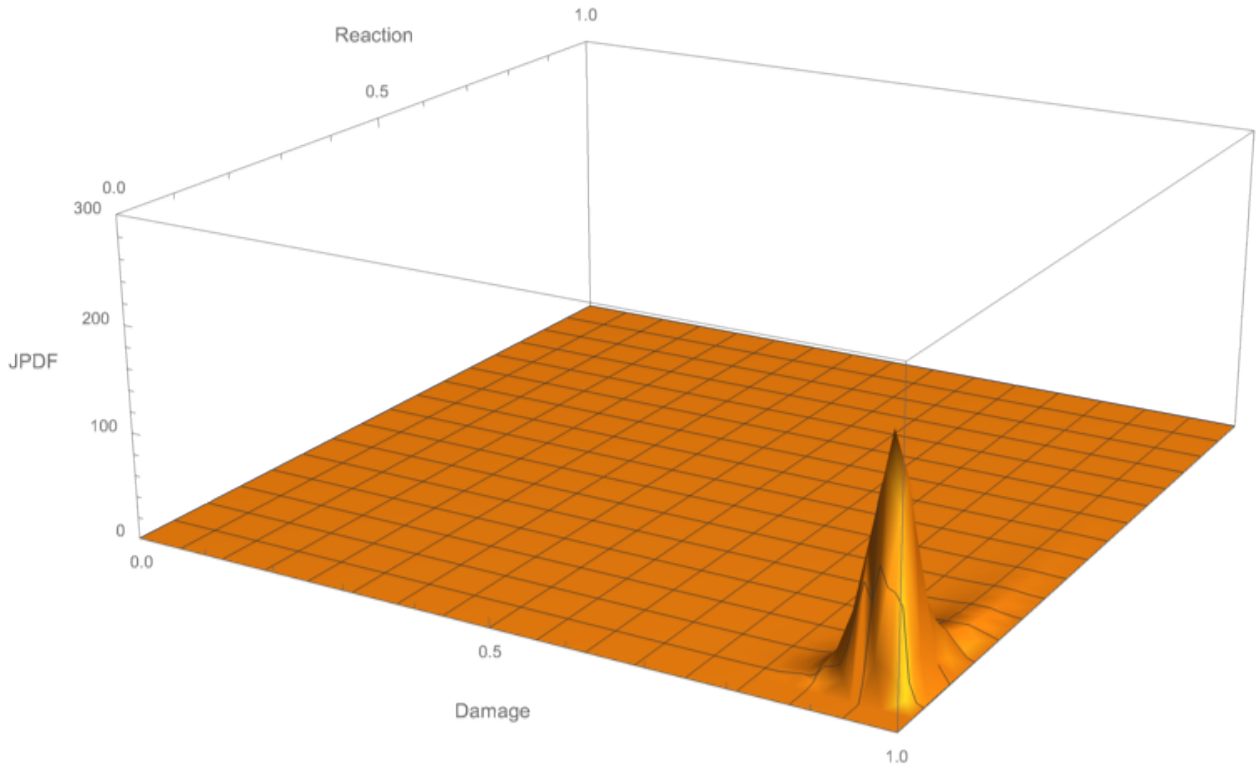

Figure 5-12. JPDF for Composition B at 79.2e-6 seconds.

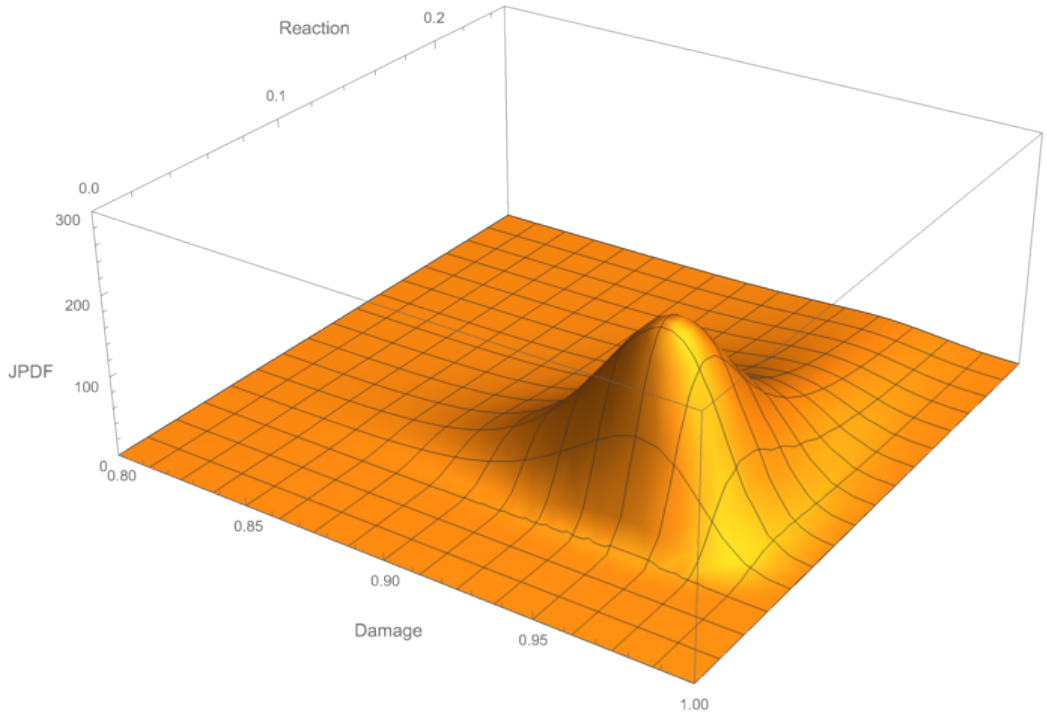

Figure 5-13. Magnified JPDF for Composition B at 79.2e-6 seconds.

A second set of analyses were performed where damage of the energetic is neglected from the solution. Once again, a statistical sample size of 100 realizations were chosen to capture the stochastic ignition of the Composition B material, therefore 100 analyses have been performed. The ignition of the energetic was once again assumed when the product gas exceeded a temperature of approximately 3500 K. The resulting mean gas temperature is shown in Figure 5-10.

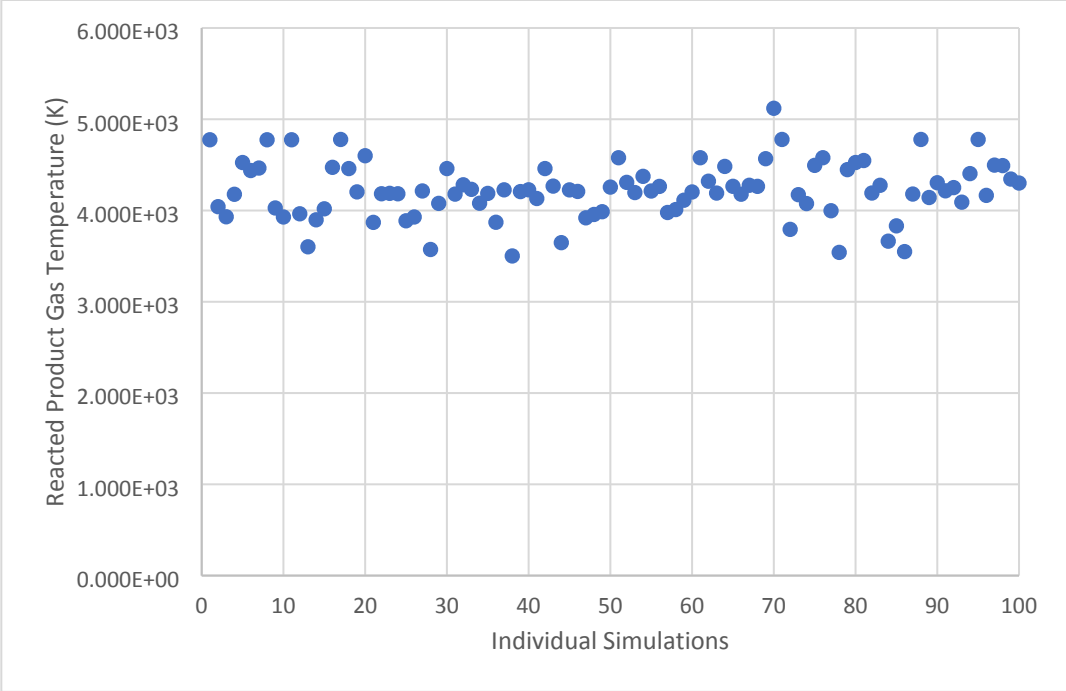

Figure 5-14. Gas Temperature at ignition of Composition B with piston velocity at 250 m/s without damage modeling.

The mean gas temperature is 4224 K at ignition and a deviation of 305 K. The resulting ignition time is shown in Figure 5-11.

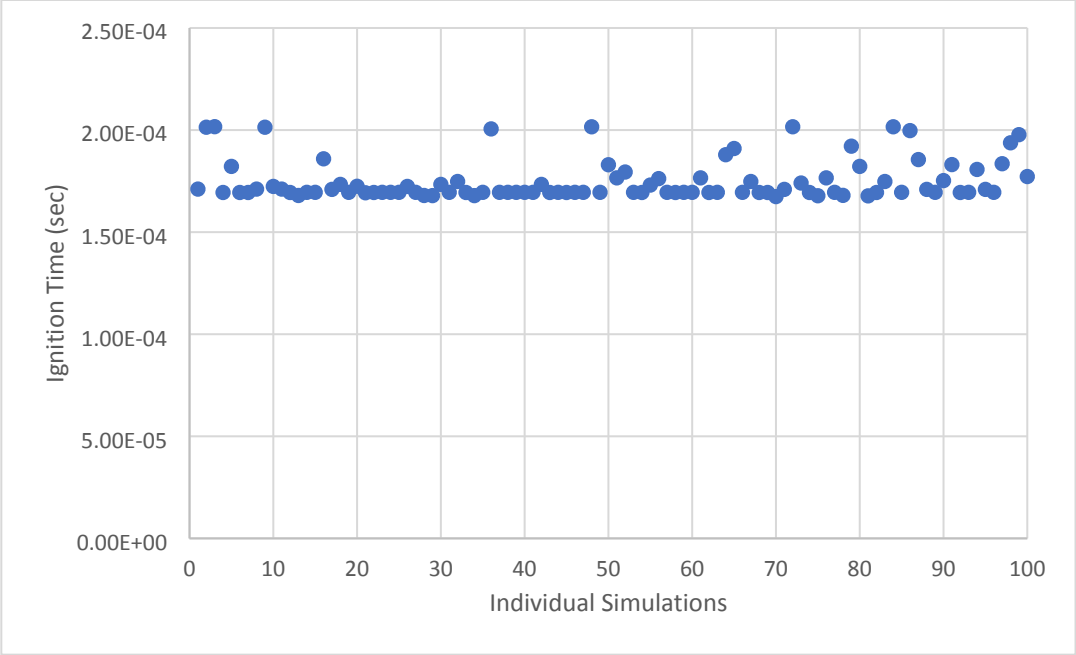

Figure 5-15. Ignition time of Composition B with piston velocity at 250 m/s without damage modeling.

The average ignition time is 1.75e-4 seconds and the deviation is 9.82e-6 seconds. The resulting ignition location is shown in Figure 5-12.

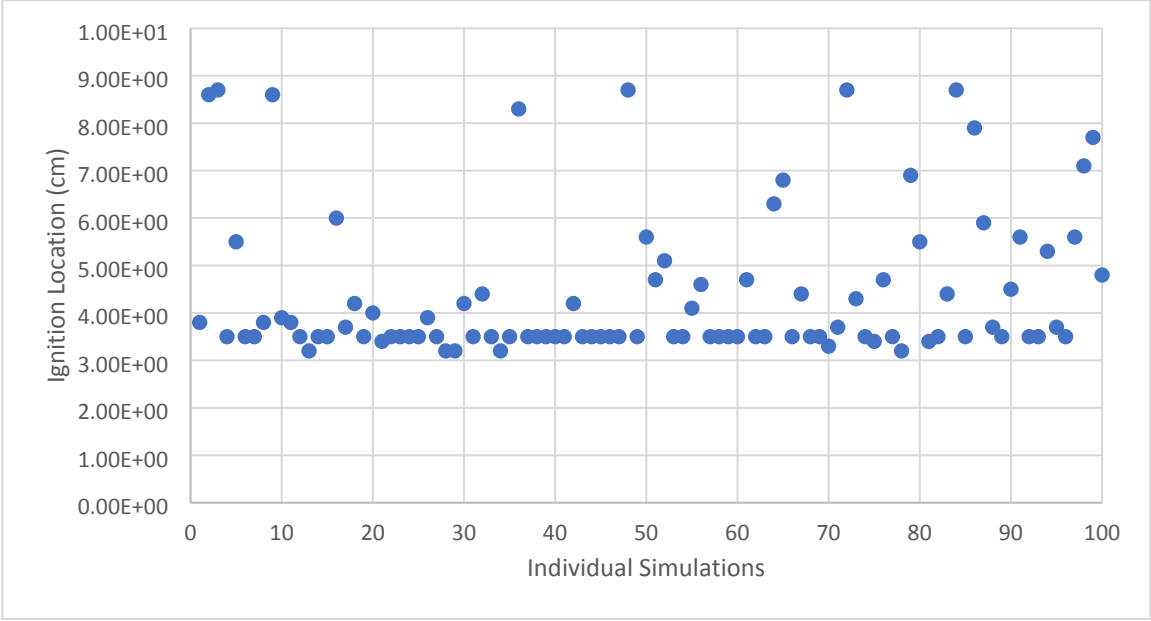

Figure 5-16. Ignition location of Composition B with piston velocity at 250 m/s without damage modeling.

The initial location front of the Composition B is at 0 cm. The average ignition location is at 4.4 cm with a deviation of 1.53 cm.

From the results above the inclusion of the damage results in an increase in the reaction rate of the energetic material resulting in a decrease to ignition time as seen by comparing Figures 5-7 and 5-11. The inclusion of damage is shown to reduce the variability in the solution as compared to the no damage solution. As damage progresses, the mass exchange rate increases due to the increasing surface area, thus reducing the time to ignition. The diffusion model used in the solution is dependent on the solution time, where more diffusion is present in the solution as the ignition time increases, see Equations 5.2.7 and 5.2.8. In addition, the diffusion model is based upon Brownian motion and the type of diffusion model chosen. As time increases the amount of diffusion increases, thus increasing the variability in ignition time and position.

This page intentionally left blank

6. CONCLUSION

In conclusion, this report discusses three stochastic modeling approaches using random variables to capture stochastic processes. The stochastic methods are based in computational shock physics coupled with a particle method to solve a set of random variables computed using Stochastic Differential Equation (SDEs). This approach applies stochastic methods to the material and/or exchange model where the SDE is used to describe effects at the microstructural length scale. The microstructural effects modeled by the stochastic processes greatly affect the outcome of an event. Examples of spallation of materials and the reaction of energetic materials has been presented. In the case of spallation, the nucleation of cracks at the microstructure length scale, coalesce forming a macrocrack. In the case of energetic reaction, energy localization at the microscopic length scale causes ignition of the energetic at the macroscopic level.

In this report, damage, temperature and/or reaction have been selected as random variables in three example applications. The collection of particles in the computational cell is used to describe the fluctuations of temperature, crack nucleation (damage) or energy localization effects (reaction). These fluctuations are captured by binning the random variables across the particle field in the computational cell. From the particle binning process, a mean and variance are computed, and these values are used to compute characteristic values of a chosen Probability Density Function (PDF). The PDF is used to compute an averaged macroscopic quantity in the computational grid cell describing the effect of the random variable on the material behavior. The choice of the random variable is one of the most critical aspects of the stochastic modeling process.

Three distinct stochastic modeling methods have been presented where each method has strengths and weaknesses. In all three methods, particles are the basis for computing a mean and variance of each random variable. The first method, is based upon a single random variable and the third method, is based upon the coupling of N-random variables. Both methods use an arbitrary diffusion model. The random variable evolves in time "arbitrarily" without the constraint of an assumed PDF on the particle. In the case of method two, the diffusion model is based upon a chosen PDF where the evolution of the random variable on the particles preserves the PDF distribution. Both the diffusion and drift models are determined based upon the PDF and the forward and backward Kolmogorov equations. Using the distribution of the random variable on the particle, the mean and variance are computed from the particle field in the computational grid cell.

All methods compute an average macroscopic quantity in the computational grid cell that describes the effect of the random variable on the material behavior. Using the mean and variance computed from the distribution of the random variable on the particle, coefficients of a PDF are computed. For method one, where the diffusion model is arbitrary, the coefficients are computed for an assumed PDF. For method two, the coefficients are computed for the PDF that defined the diffusion model. For method three, the coefficients for the marginals from the Joint Probability Distribution Function (JPDF) are computed. Using the PDF or JPDF, an averaged macroscopic material property or material state is computed.

Lastly, as the choice of the random variable is one of the most critical steps, choosing the PDF or JPDF is also one of the most critical steps of the stochastic modeling process. The choice may be determined several ways and two examples are meso/microscale analysis and experimental data.

REFERENCES

[1] Baer, M. R. Gartling, D. K. and DesJardin, P. E., Probabilistic Models for Reactive Behavior in Heterogeneous Condensed Phase Media, Combustion Theory and Modeling, 16:1, 75-106, DOI: 10.1080/13647830.2011.606916

[2] Maymon, Giora, Stochastic Crack Propagation, Elsevier Academic Press, ©2018

[3] Chu, Shanshan, Guilleminot, Johann, Cambre, Kelly, Bijan, Abar, Gall, Ken, Stochastic modeling and identification of material parameter on structures produced by additive manufacturing, Comput. Methods Appl. Mech. Engrg, 387, 2021, 114166

[4] Ostoja-Starzewski, M., Random Field Models of Heterogenous Materials, Int. J. Solid Structures, Vol. 35, No 19, pp. 2429-2455

[5] Williams, Todd O., A Stochastic Transformation Field Theory for Heterogenous Materials, J. Engng. Mech. DOE: 10.1061/(ASCE)0733-9399(2006)132:11(1224)

[6] Pope, S.B., Lagrangian PDF Methods for Turbulent Flows, Annu. Rev. Fluid Mech. 1994, 26, pp. 23-63.

[7] Schumacher, S. C. and Baer, M. R., Generalized Continuum Mixture Theory for Multi-Material Shock Physics, SAND2021-15661

[8] Kittell, David E., Yarrington, Cole D., Lechman, Jeremey B., Knepper, Robert, Bolintineanu, Dan S., Shand, Lyndsay, Damm, David L. and Olles, Joseph D., Pushing Continuum Reactive Capabilities through Novel Sub-Grid and Statistical Methods, SAND2019-11891

[9] Hertzler, Greg, A Stochastic Differential Equation for Modeling the "Classical" Probability Distributions, 47th Annual Conference of the Australian Agricultural and Resource Economic Society, Fremantle, Western Australia, 12-14 Feb 2003

[10] Gumbel, E.J., Bivariant Exponential Distributions, Journal of the American Statistical Association, June 1960, Vol. 55, No.294, pp. 698-707

[11] Gumbel, E.J., Bivariant Logistic Distributions, Journal of the American Statistical Association, June 1961, Vol. 56, No.294, pp. 335-349

[12] Balakrishan, N. and Lai, Chin-Diew, Continuous Bivariate Distributions, Springer, ©2009, 2nd Edition

[13] Kolmogorov, Andrei, Uber die analytischen Methoden in der Wahrscheinlichkeitstheorie, Mathematische Annalen, 104, pp. 415-458. doi:10.1007/BF01457949 (German).

[14] Osendal, B., Stochastic Differential Equations, Springer Science and Business Media, 2003.

[15] Schumacher, S. C. and Bardenhagen, S., Marker Technologies in a Generalized Continuum Mixture Theory for Multi-material Shock Physics, draft.

[16] Schumacher, S. C., User Manual-Generalized Continuum Mixture Theory for Multi-material Shock Physics, draft.

[17] Hansen, Andrew C and Baker-Jarvis, James, A Rate Dependent Kinetic Theory of Fracture for Polymers, International Journal of Fracture, 44 pps 221-231, 1990

[18] Baer, M. R., A Stochastic "Hot-Spot" Model, White paper.

[19] Schumacher, S. C. and Baer, M. R., Calibration of a Reactive Flow Model for Bullseye, SAND2021-12798

[20] Baer, M.R. and Trott W. M., Mesoscale description of shock-loaded heterogenous porous material, Shock Compression of Condensed Matter-2001, AIP Proceeding, 620, pp.713-716.

[21] Thompson, Darla G. and LeLuca, Racci, Time-Temperature Analysis Applied to Mechanical Properties Data from a Wide Variety of Plastic Bonded Explosive Formulations, LA-CP-13-01080

DISTRIBUTION

Email—Internal

Name	Org.	Sandia Email Address
Kyran Mish	1555	kdmish@sandia.gov
Daniel Rogers	1555	dnrogers@sandia.gov
Russell Teeter	1555	rdteete@sandia.gov
Devon Dalton	6632	ddalton@sandia.gov
Todd Miner	6647	rtminer@sandia.gov
Antonio Garcia	6647	argarc@sandia.gov
Technical Library	1911	sanddocs@sandia.gov

This page left blank

Sandia National Laboratories

Sandia National Laboratories is a multimission laboratory managed and operated by National Technology & Engineering Solutions of Sandia LLC, a wholly owned subsidiary of Honeywell International Inc. for the U.S. Department of Energy's National Nuclear Security Administration under contract DE-NA0003525.